Holocene thinning and grounding-line retreat of Darwin and Hatherton Glaciers, Antarctica

Trevor R. Hillebrand[1*], John O. Stone[1], Michelle Koutnik[1], Courtney King[2], Howard Conway[1], Brenda Hall[2], Keir Nichols[3], Brent Goehring[3], Mette K. Gillespie[4]

[1]Department of Earth and Space Sciences, University of Washington, Seattle, WA 98195, USA
[2]Laboratory School of Earth and Climate Science and Climate Change Institute, University of Maine, Orono, ME 04469, USA
[3]Department of Earth and Environmental Sciences, Tulane University, New Orleans, LA 70118, USA
[4]Faculty of Engineering and Science, Western Norway University of Applied Sciences, Sogndal, 6856, Norway
[*]Now at Fluid Dynamics and Solid Mechanics Group, Los Alamos National Laboratory, Los Alamos, NM 87545, USA

Correspondence to: Trevor R. Hillebrand (trhille@lanl.gov)

Abstract. We present exposure ages of glacial deposits at three locations alongside Darwin Glacier and its tributary Hatherton Glacier that record several hundred meters of late Pleistocene to early Holocene thickening relative to present. As the grounding-line of the Ross Sea Ice Sheet retreated rapidly southward, Hatherton Glacier thinned steadily from about 9 kyr BP until about 3 kyr BP. Our data are equivocal about the maximum thickness and mid-to-early Holocene history at the mouth of Darwin Glacier, allowing for two possible deglaciation scenarios: (1) ~500 m of steady thinning from 9 kyr BP to 3 kyr BP, similar to Hatherton Glacier, or (2) ~950 m of thinning, with a rapid pulse of ~600 m thinning at around 5 kyr BP. We test these two scenarios using a 1.5-dimensional flowband model of Darwin and Hatherton Glaciers, forced by ice-thickness changes at the mouth of Darwin Glacier and evaluated by fit to the chronology of deposits at Hatherton Glacier. Our modeling shows that the constraints from Hatherton Glacier are consistent with the interpretation that the mouth of Darwin Glacier thinned steadily by ~500 m from 9 kyr BP to 3 kyr BP; rapid pulses of thinning at the mouth of Darwin Glacier are ruled out by the data at Hatherton Glacier. This contrasts with some of the available records from the mouths of other outlet glaciers in the Transantarctic Mountains, many of which thinned by hundreds of meters over roughly a one-thousand-year period in the early Holocene. The deglaciation histories of Darwin and Hatherton Glaciers are best matched by a steady decrease in catchment area through the Holocene, suggesting that Byrd and/or Mulock glaciers may have captured roughly half of the catchment area of Darwin and Hatherton Glaciers during the last deglaciation. An ensemble of three-dimensional ice-sheet model simulations suggest that Darwin and Hatherton Glaciers are strongly buttressed by convergent flow with ice from neighboring Byrd and Mulock glaciers, and by lateral drag past Minna Bluff, which could have led to a pattern of retreat distinct from other glaciers throughout the Transantarctic Mountains.

1 Introduction

Quaternary glacial deposits preserved in ice-free regions around the Darwin-Hatherton glacier system (DHGS) have been used to infer the glacial history of the region (Bockheim et al., 1989; Conway et al., 1999; Storey et al., 2010; Joy et al., 2014; King et al., 2020). In this paper, we present new geologic and exposure age results from Hatherton and Darwin Glaciers and use

these data to constrain a 1.5-D glacier flowband model of the DHGS to interpret these ages in terms of ice thickness near the glacier mouth from the Last Glacial Maximum (LGM) to present. We then present an ensemble of 10 km-resolution simulations of the last deglaciation in the Ross Embayment using the Pennsylvania State University (PSU) 3-D ice sheet model (Pollard & DeConto, 2009; 2012) to determine what these local results might suggest about large-scale ice dynamics in the region.

1.1 The Last Deglaciation in the Ross Embayment

Grounded ice filled the Ross Embayment of Antarctica during the last glaciation (~20 – 14 kyr BP) (Figure 1). The grounding-line of this Ross Sea Ice Sheet retreated more than 1,200 km along the western side of the embayment to its current position, from 13 to 2 kyr BP (Anderson et al., 2014). Conway et al. (1999) contrasted this with the persistence of grounded ice over Roosevelt Island until the late Holocene, and thus proposed that grounding-line recession followed the pattern of a swinging gate, with its hinge in the eastern Ross Sea (Figure 1). Initial radiocarbon ages from deposits alongside Hatherton Glacier (Bockheim et al., 1989) suggested that the glacier had reached its modern configuration >6.8 kyr BP, which provided one of the key constraints for this model of grounding-line retreat.
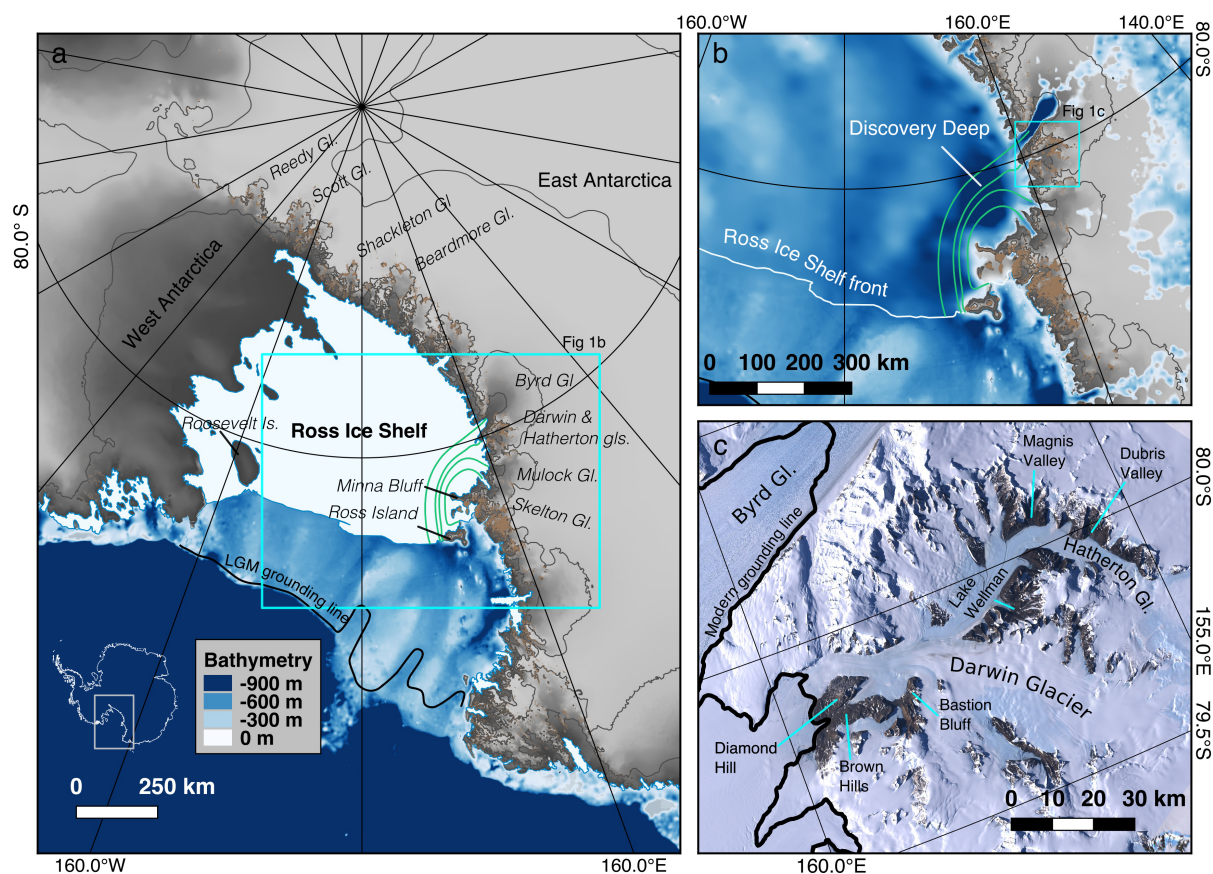
Figure 1: **a** The Ross Embayment of Antarctica, with regional and study locations noted. The modern ice sheet surface is
shown in grey, the modern ice shelf is shown in white and exposed rock is shown in brown. Bathymetry beyond the Ross Ice
Shelf front is shown in blues (Fretwell et al., 2013). LGM grounding line from Halberstadt et al. (2016). Flowlines through
the ice shelf from Byrd, Darwin, Mulock, and Skelton glaciers are shown in green, and calculated using the MATLAB toolbox
of Greene et al. (2017). **b** Inset of area outlined with cyan box in panel A, with bathymetry shown in the same colormap as
panel A. The Ross Ice Shelf has been removed to show bathymetry. The combined Byrd-Darwin-Mulock-Skelton flow path
covers Discovery Deep, which is the deepest part of the seafloor in the Ross Embayment. **c** Landsat imagery of Darwin and
Hatherton Glaciers, with labels for locations mentioned in the text (Bindschadler et al., 2008). The modern grounding line is
shown by the thick black line. Note the prominent blue-ice fields on the glacier surfaces.

More recent data show that the ~800 km-long section of the Transantarctic Mountains (TAM) front between Terra Nova
Bay and Shackleton Glacier may have deglaciated almost simultaneously in the early Holocene, followed by slow recession
into the late Holocene (Spector et al., 2017). Lower Shackleton and Beardmore Glaciers had reached their modern
configurations by 7.4 kyr BP, roughly contemporaneous with dramatic thinning at Mackay Glacier (Jones et al., 2015) and
evidence of ungrounding of ice in McMurdo Sound (Hall et al., 2004). The pattern of deglaciation was likely complex, as the
grounding-line temporarily stabilized on pinning points and retreated in deep troughs (Dowdeswell et al., 2008; Halberstadt et
al., 2016). After ~7 kyr BP ice sheet thinning in the southern Ross Embayment slowed as the grounding-line neared its modern
position between Scott and Reedy glaciers around 3 kyr BP (Spector et al., 2017).

1.2 Physiographic setting of Darwin and Hatherton Glaciers

Darwin Glacier and its major tributary Hatherton Glacier are outlets of the East Antarctic Ice Sheet that flow through the
TAM into the modern Ross Ice Shelf. In contrast to the neighboring fast-flowing and much larger Byrd and Mulock glaciers,
ice-flow velocities for the DHGS do not exceed 110 m yr^{-1}, and everywhere the velocity of Hatherton Glacier is <12 m yr^{-1}
(Rignot *et al.*, 2011; Gillespie *et al.*, 2017). The catchment for the DHGS is small (8060 km^2) due to both high bedrock
topography preventing flow into their canyons and to the proximity of the much larger Byrd and Mulock glaciers, whose
catchments effectively cut off the Darwin-Hatherton catchment (Swithinbank *et al.*, 1988; Gillespie *et al.*, 2017). While Byrd
and Mulock glaciers currently contribute about 22 and 5 Gt a^{-1} to the Ross Ice Shelf, respectively (Stearns, 2011), Darwin
Glacier contributes 0.24 ± 0.05 Gt a^{-1} (Gillespie et al., 2017). The modern grounding-line of Darwin Glacier sits on a forward
sloping bed ~925 m below sea level (Gillespie et al., 2017).

The surface mass balance of the DHGS is spatially complex, with persistent blue ice areas and seasonal surface melt (Brown
and Scambos, 2004; Gillespie et al., 2017). Net ablation is evident alongside the glaciers, which are bordered by the largest
area of exposed rock in the TAM outside of the Dry Valleys/McMurdo Sound region, exceeding 800 km^2. The boundary layer
meteorology is dominated by strong, dry, and cold downslope winds between April and September, with mean monthly air
temperatures around -25°C (Noonan *et al.,* 2015). In December and January, relatively humid winds dominate, and mean

monthly temperatures rise to -4°C. Blue ice areas occur where katabatic winds converge beneath zones of turbulence in the lee of mountains and nunataks (Bintanja, 1999). Therefore, most ablation likely occurs during the winter months, due to removal of surface snow by strong downslope winds, although surface meltwater is visible in the summer (e.g., Kingslake et al., 2017).

85   Brown and Scambos (2004) showed that blue ice areas on Darwin Glacier are likely very near their maximum extent, and only small climate fluctuations are required to greatly reduce their area. Of the available surface mass balance products, only the 5.5 km RACMO 2.1 product (Lenaerts et al., 2012a) predicts an overall mass balance close to that calculated from field measurements (Gillespie et al., 2017).

Seasonal ablation and localized melting have produced numerous lakes and ponds that are found at the edges of Darwin
90   and Hatherton glaciers, including large frozen lakes at the glacier margins, seasonal supraglacial ponds at low elevations, and isolated ponds around Diamond Hill. While some of the larger lakes could be frozen through to their beds, the ice-shelf dammed Lake Wilson is capped by floating ice, with a stratified water column ~100 m deep (Hendy, 2000; Webster et al., 1996). All of these environments host modern blue-green algae (cyanobacterial mats), which are the living equivalents of the freeze-dried algae material preserved within glacial deposits and described by Bockheim et al. (1989) and King et al. (2020).

95   Farther downstream within the Ross Ice Shelf, ice from the DHGS converges with ice from Byrd and Mulock glaciers (Figure 1). The convergence occurs over 'Discovery Deep', the deepest part of the Ross seafloor on the continental shelf (up to ~1300 m below sea level). Thomas et al. (1984) inferred positive vertical strain rates along this flow path south of Minna Bluff, which they attributed to the convergence of flow from Byrd, Mulock, Darwin, and Skelton glaciers, combined with the influence of Minna Bluff. Whillans and Merry (2001) also identified Minna Bluff and Cape Crozier as obstacles that provide
100 stabilizing backpressure to the Ross Ice Shelf and cited the presence of rifts at the tip of Minna Bluff as evidence of stress concentration on the upstream side. Hughes et al. (2017) posited that Byrd Glacier effectively buttresses ice from West Antarctica by "nailing" the Ross Ice Shelf to the TAM and reducing extensional strain rates in the ice shelf. In their analysis, without the presence of Byrd Glacier, the Ross Ice Shelf would deform along the TAM front with minimal side shear stress to resist flow. Mulock Glacier adds to this effect by exerting pressure on Byrd in opposition to West Antarctic Ice. While Darwin
105 Glacier is extremely small compared to Byrd and Mulock, it is the only one of the three to have well-documented and extensive glacial deposits. If the hypothesis of Hughes et al. (2017) is correct, the history of ice dynamics in the Byrd-Darwin-Mulock-Skelton region may be key to understanding the dynamics of grounding-line retreat in the Ross Embayment during the last deglaciation, and possibly to the stabilization of the grounding line of the West Antarctic Ice Sheet.

1.3 Late Pleistocene-Holocene growth and retreat of the Darwin-Hatherton Glacier System

110 During the last glaciation, other outlet glaciers throughout the TAM thickened initially at their mouths in response to grounded, thickening ice in the Ross Sea, and later upstream due to increased accumulation after the LGM (Todd et al., 2010). Lateral moraines formed during this period have been used to interpret ice thicknesses of both the grounded ice sheet in the Ross Sea and the EAIS outlet glaciers (Bockheim et al., 1989; Bromley et al., 2010, 2012; Denton et al., 1989; Hall et al., 2015; Jones et al., 2015; Joy et al., 2014; Spector et al., 2017; Todd et al., 2010).

115 Bockheim et al. (1989) mapped lateral moraines and drift sheets in ice-free valleys alongside Hatherton Glacier, and dated these deposits based on weathering, soil characteristics, and radiocarbon ages of freeze-dried algae. These algae grew in glacier-dammed ponds and died when the ponds disappeared as the glacier retreated downslope; the radiocarbon ages of the algae provide a proxy for the glacier margin position through time (Bockheim et al., 1989; King et al., 2020). Bockheim et al. (1989) distinguished five drift units: Hatherton, Britannia-I, Britannia-II, Danum, and Isca Drifts, in order from youngest to

120 oldest. All subsequent work has adopted these names and confirmed the original mapping. Although we mapped and sampled some material from the three oldest deposits, this paper focuses on the Britannia-I and Hatherton Drift.

The chronology and correlation of these deposits along the Hatherton-to-Darwin Glacier flowline remains uncertain, and the Britannia-II, Britannia-I and Hatherton Drifts have each been identified with the last maximum glaciation in this sector of the TAM (Bockheim et al., 1989; Storey et al., 2010; Joy et al., 2014; King et al., 2020). In addition to determining which

125 deposits represent the last local maximum, projection of the associated ice surface downstream from sites on Hatherton Glacier to the surface of the Ross Sea Ice Sheet has been complicated by the absence of comparable deposits on Diamond Hill at the glacier mouth. The ice surface elevation at the outlet of Darwin Glacier is key to understanding the dynamics of grounded LGM ice south of Ross Island, and is likely a pointer to the behavior of much larger Byrd and Mulock Glaciers, which dominate ice flow into this region.

130 Although Bockheim et al. (1989) tentatively attributed Britannia-II drift to the LGM, and Britannia-I deposits to a Holocene still-stand or re-advance, Joy et al. (2014) have since dated Britannia-II drift to the penultimate glacial maximum. Younger and fresher Britannia I drift occurs up to ~350 m above the modern margin of Hatherton Glacier in Dubris and Bibra Valleys, Magnis Valley and at Lake Wellman (Bockheim et al., 1989; Storey et al., 2010; Joy et al., 2014; King et al., 2020). At these sites, the deposit is a boulder and cobble-rich ablation till, with clasts showing varying degrees of weathering. Large but

135 discontinuous ice-cored moraines mark the limit of the deposit at Lake Wellman and in Magnis Valley, and separate it from the older Britannia-II drift. At Dubris and Bibra Valleys the LGM limit varies from a thin scatter of fresh clasts to a low ridge of cobbles and boulders lacking an ice core. Clasts are distinctly less weathered than those in the underlying Britannia-II drift. Similar recessional drift extends from the Britannia-I limit towards the present glacier margin, including low moraine ridges and numerous relict lake-ice boulder pavements (King et al., 2020).

140 The Hatherton drift is a minimally weathered deposit, commonly underlain by relict ice, and found within 50 – 100 m elevation of the modern margin of Hatherton Glacier. While Bockheim et al. (1989), Storey et al., (2010), Joy et al., 2014, and King et al. (2020) agree on the general characteristics of Hatherton drift, their interpretations of its significance differ. Bockheim et al. (1989) posited that Hatherton drift represents the last episode of thinning from the high-stand represented by the Britannia deposits. In contrast, Storey et al. (2010) interpreted Hatherton drift to represent the last local advance of

145 Hatherton Glacier, which they dated to 15-19 kyr BP. In making this interpretation, they discarded several younger ages of <3 kyr BP, attributing these to recent exhumation from the deposit.

Following King et al. (2020), and based on its position between Britannia-I deposits and the modern glacier, we interpret the Hatherton drift as the youngest recessional deposit along Hatherton Glacier. Differences in morphology, and the common

150 presence of an ice core and intermittent moraine along its margin suggest that the deposit marks a brief stillstand during glacial retreat, though there is no indication in the chronologies discussed below of a prolonged pause or readvance.

Given the absence of recognizable Britannia deposits at Diamond Hill, Bockheim et al. (1989) extrapolated their elevations from sites up-glacier to infer a thickening of 1100 m at the confluence of Darwin Glacier with the Ross Ice Sheet during the last glaciation; however, this was based on the assumption that the Britannia II drift represented the LGM limit, which Joy et al. (2014) showed to be incorrect. Subsequent numerical modeling experiments (Anderson et al., 2004) yielded a more modest 155 800 m of thickening relative to present, although they had to infer the bed topography by mass conservation. The inference by Storey et al. (2010) that Hatherton rather than Britannia I drift marks the LGM high-stand of Hatherton Glacier led these authors to propose no more than ~50 m of LGM thickening. King et al. (2020) were able to date the advance and retreat of Hatherton Glacier in the Lake Wellman valley using radiocarbon dating of freeze-dried algae. They showed that the glacier advanced to the Britannia-I limit at 9.5 kyr BP, and argued that both the majority of their own exposure ages and those of 160 Storey et al. (2010) were overestimates due to prior exposure of the samples. Joy et al. (2014) dated deposits in Dubris and Bibra Valleys alongside the upper Hatherton Glacier with cosmogenic ^{10}Be and ^{26}Al. They showed that Britannia II drift is in fact a deposit of the penultimate glaciation, and obtained Holocene ages similar to those of King et al. (2020) from recessional positions in Britannia I drift.

Our goals in this paper are to: (i) Extend and tie together the chronology of Britannia I and Hatherton Drift with new 165 exposure ages from Dubris, Bibra and Magnis Valleys on upper Hatherton Glacier (Figure 1), and (ii) Determine the LGM thickness and recessional history of the grounded Ross Sea Ice Sheet at the mouth of Darwin Glacier, using a combination of in-situ-produced ^{14}C exposure ages from Diamond Hill and numerical modeling of Darwin and Hatherton Glacier. We then explore the sensitivity of ice at the mouth of Darwin glacier to changes of the Ross Sea Ice Sheet using an ensemble of ice sheet model simulations.

170 2 Records of glacier fluctuations

2.1 Geochronological methods

We measured ^{10}Be and ^{26}Al in erratics we collected from Diamond Hill, as well as from Bibra, Dubris and Magnis Valleys. We selected the freshest available samples, targeting rocks with differentially weathered top and bottom surfaces, interpreted as indicating that a sample had remained stable since deposition. Collection of isolated erratics rather than from moraines 175 avoids samples which may have been disturbed, overturned, or temporarily covered during sublimation and collapse of ice in the moraine core. This process can take thousands of years in Antarctica, where some glacial maximum moraines remain ice-cored up to the present day (including those in Magnis Valley and at Lake Wellman). On the floors of Dubris, Bibra and Magnis Valleys we collected samples from Britannia and Hatherton Drift. Where it was possible, we attempted to sample areas of thin or discontinuous drift, targeting rocks resting on underlying older, consolidated drift, though the thickness of Britannia-180 I recessional deposits on the floors of Bibra and Dubris Valleys, in particular, made this difficult. A second potential

complication for these samples is coverage by proglacial lakes at the ice margin during retreat. The pervasive occurrence of sub-fossil algae (desiccated fragments of lacustrine cyanobacterial mats), discontinuous shorelines, and lake-floor pavements in both valleys indicates that retreating ice was fronted by one or more shallow proglacial lakes throughout deglaciation. Although we sampled to avoid cover by lakes, some valley floor exposure ages may have been affected and therefore

185   underestimate depositional ages. We also noted the relative height of nearby boulders and the dominant orientation of local snow tails so as not to sample rocks that may have been covered by drift snow. In these wind-swept areas adjacent to blue ice glacier margins, it is unlikely that deep snow cover would persist for long enough to strongly skew the exposure ages.

We also measured cosmogenic ^{14}C produced *in situ* in quartz along an elevation transect of granitic bedrock from Diamond Hill to constrain the LGM ice thickness. We preferentially sampled very weathered bedrock to ensure minimal erosion over

190   the last glacial cycle. Because any rock exposed during the few tens of kyrs prior to the LGM may contain inherited ^{14}C, apparent ^{14}C exposure ages provide an upper bound on the timing of exposure since the LGM. However, the short half-life of ^{14}C makes these exposure ages less sensitive to exposure prior the LGM than ^{26}Al or ^{10}Be ages. Within the range of subaerial erosion rates typical of Antarctic bedrock (<1 m/Myr), ^{14}C concentrations reach secular equilibrium in ~30 kyr (Balco et al., 2016). Because of the short half-life of ^{14}C, a few thousand years of ice cover during the LGM will create a detectable signal

195   of burial, while rock that was not covered by ice in the last 30 kyr will remain at its equilibrium concentration. Our goal at Diamond Hill, where there are no deposits that indicate the upper limit of glacial maximum ice cover, was to bracket LGM ice elevation between the lowest sample that is saturated with respect to ^{14}C (i.e., not ice-covered during the LGM) and the highest unsaturated sample (i.e., ice-covered during the LGM).

We used conventional purification methods including heavy liquid separation, surfactant separation, and dilute HF etching

200   at ~60°C (Kohl and Nishiizumi, 1992) to isolate pure quartz for exposure dating. Samples analyzed for *in-situ* ^{14}C were prepared and measured twice. For the first set, quartz purified at UW was further treated at the Tulane lab with 1:1 concentrated HNO$_3$:de-ionized water for 30 minutes at room temperature prior to loading into the carbon-extraction system. Following a 500°C pre-heating *in vacuo*, ^{14}C was extracted using methods described by Goehring et al. (2019). Five of the six samples in this first batch gave ^{14}C concentrations exceeding theoretical saturation concentrations (by up to ~75%). Realizing that this

205   was due to contamination by modern carbon from residual surfactant-separation reagents that survived the procedures described above, we re-analyzed all six samples using a more aggressive pre-treatment protocol, as described by Nichols and Goehring (2019). Results reported in this paper are from this second set of analyses; the results from the first set are reported by Nichols and Goehring (2019). As a further check on the validity of the second set of measurements, we also analyzed two erratic samples from Diamond Hill and Danum Platform, which gave exposure ages in agreement with ^{10}Be and ^{26}Al results.

210   Complete analytical results are given in the supplementary information. We isolated Be and Al for isotopic analysis at the University of Washington Cosmogenic Nuclide Laboratory following the standard ion-exchange chromatography method of Ditchburn and Whitehead (1994). ^{14}C cathodes were prepared at Tulane University using the new fully-automated carbon extraction and graphitization system (Goehring et al., 2019a).

215 We analyzed samples for *in situ* ^{10}Be at the Center for Accelerator Mass Spectrometry (CAMS) at Lawrence Livermore National Laboratory. As a further check, we analyzed ^{26}Al from the same aliquots of quartz at the Purdue Rare Isotope Measurement Laboratory (PRIME). ^{14}C cathodes were analyzed at the National Ocean Sciences Accelerator Mass Spectrometry Laboratory and the Woods Hole Oceanographic Institution. The exposure ages presented in this paper have been calculated using the latitude-altitude scaling scheme of Stone (2000). While the choice of another scaling scheme changes the individual exposure ages, there is no major impact on the overall results, and we have therefore chosen to present results based

220 on this scheme for simplicity.

Sample data and calculated ages for all samples in this study are found in the Supplemental Material and are archived at ice-d.org.

2.2 Chronology of glacial deposits

2.2.1 Dubris and Bibra Valleys

225 The Britannia I limit across Dubris and Bibra Valleys (Figure 2) represents at least 370 m of thickening relative to the present Hatherton Glacier surface, and dates to 8-10 kyr BP (Figure 3). Slight variations in the age of the Britannia I limit between different sites is to be expected, as changes in local meteorology could allow small-scale fluctuations of the ice margin. After 8 kyr BP, the glacier margin began to retreat steadily towards its present position. Only one exposure age exhibits significant prior exposure to cosmic rays (13-HAT-133-BV; 79 kyr). This sample was the closest to the glacier margin, and thus prevents

230 us from better constraining the last 150 m of glacier thinning. The thinning profile on Danum Platform is steeper than in Dubris and Bibra Valleys, which could be an effect of either the complex topography or lake cover in the valleys.
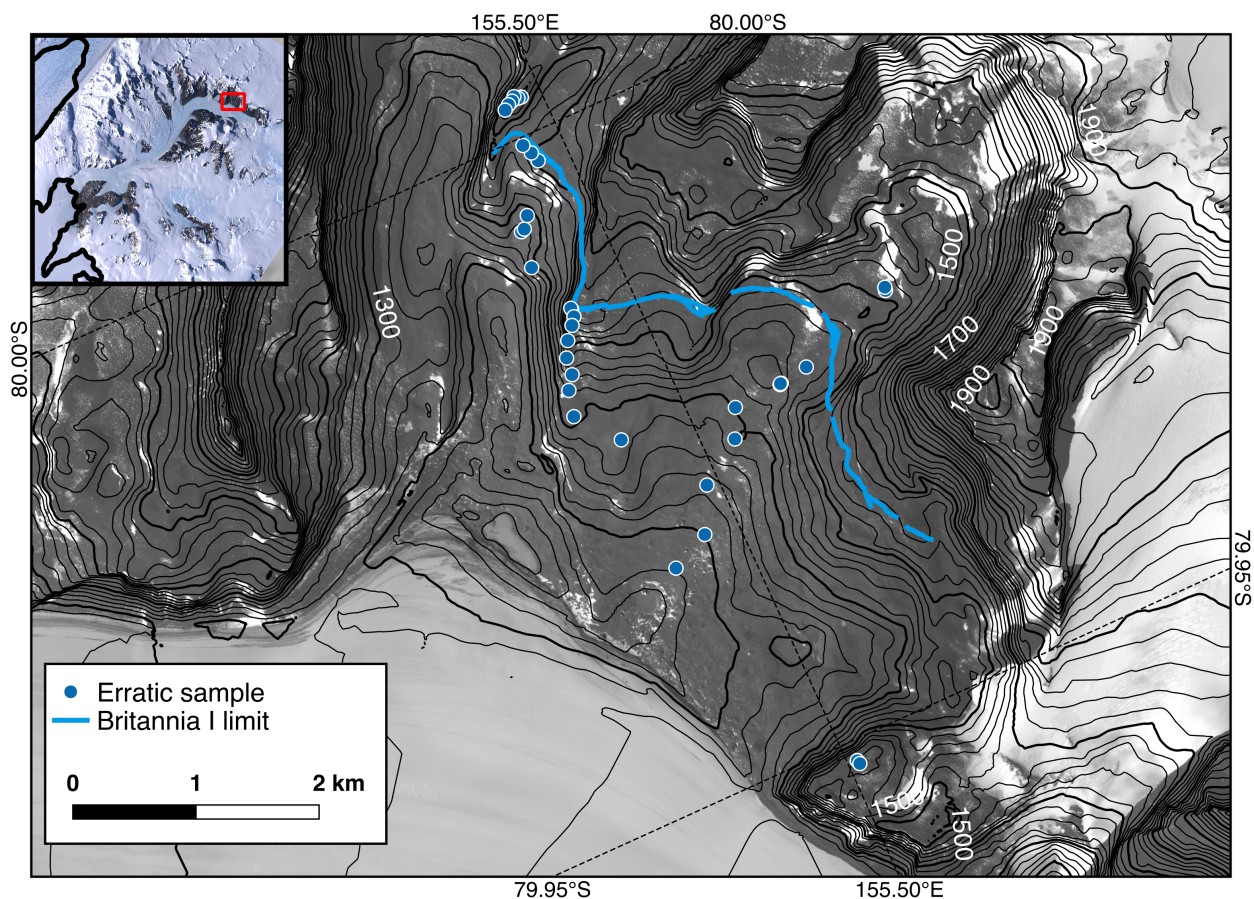
Figure 2: Simplified map of Dubris and Bibra Valleys, showing sample locations and elevations shown in 20 m contours (100 m contours are in bold). The blue curve represents the Britannia I limit; erratic samples outboard of that limit are taken from the limit of the older Britannia II deposit. Contours and satellite imagery from Land Information New Zealand (LINZ, 2010). Inset imagery from Bindschadler et al. (2008).
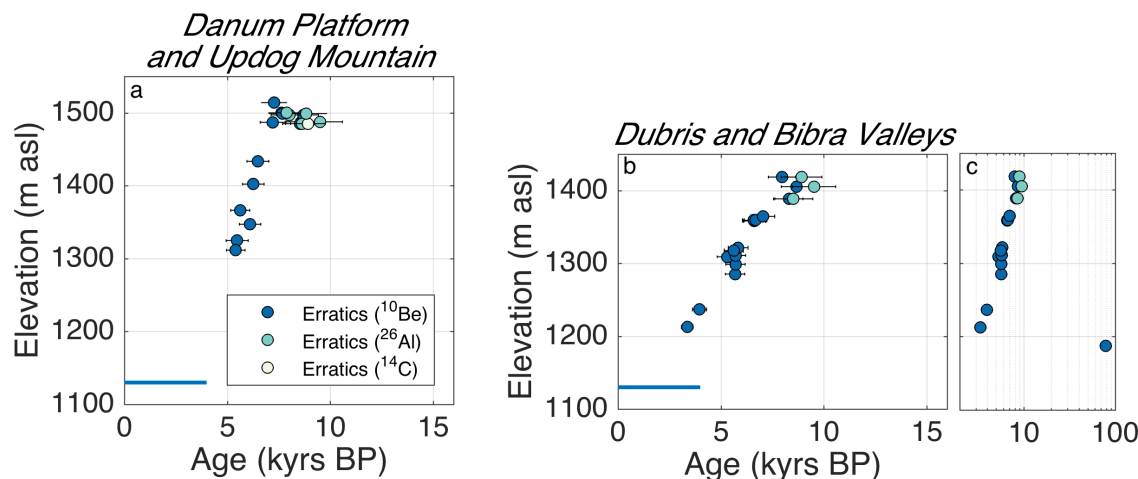
Figure 3: Surface exposure ages of glacial erratics from atop bedrock platforms (**a**) and Dubris and Bibra Valleys (**b**), showing a stable margin until 7-8 kyr BP, after which the glacier thinned steadily towards its modern configuration. Horizontal blue line shows elevation of present-day glacier margin. Panel c shows all surface exposure ages of the Britannia I deposit in Dubris and Bibra Valleys on a logarithmic scale to include one sample with significant inherited nuclides.
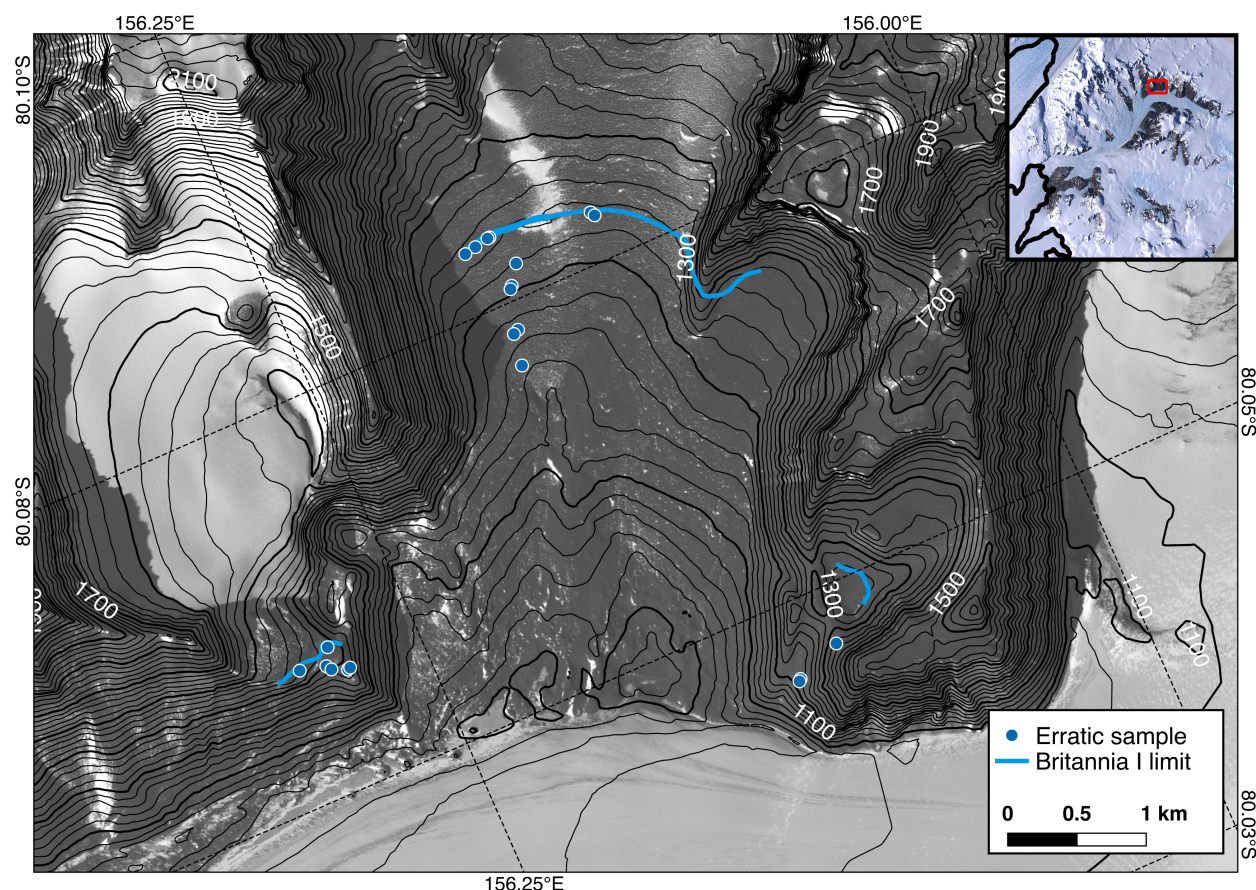
2.2.2 Magnis Valley

The Britannia I limit in Magnis Valley (Figure 4) predates the limit at Dubris and Bibra Valleys, with ages spanning 7.8 – 13.9 kyr on the valley walls, and 8.3 – 12.4 kyr on the valley floor (Figure 5). A single pre-exposed sample at the drift limit dates to ~32 kyr BP. Ignoring this one date, if the ages at the upper end of these distributions are valid and not due to small degrees of prior exposure, they imply that the glacier margin was close to its limit in Magnis Valley for ~ 6 kyr. At Lake Wellman, ^{14}C ages of subfossil algae suggest that the glacier margin there advanced by ~ 500 m (50 m in altitude) from 13 - 11 kyr BP (King et al., 2020). Differences between the apparent ages and durations of maximum advance at Bibra, Dubris and Magnis Valleys and at Lake Wellman may reflect small-scale differences in microclimate between the sites, or may be an artifact of having dated too few samples at each site to constrain the full span of each maximum advance. Based on flowline modeling in Section 3 that suggests there should not be significant time lags between advances at these sites along Hatherton Glacier, we view the data cumulatively and infer that Hatherton Glacier was close to maximum thickness from at least ~14 kyr BP until ~8 kyr BP, although there is considerable variation in timing between sites.
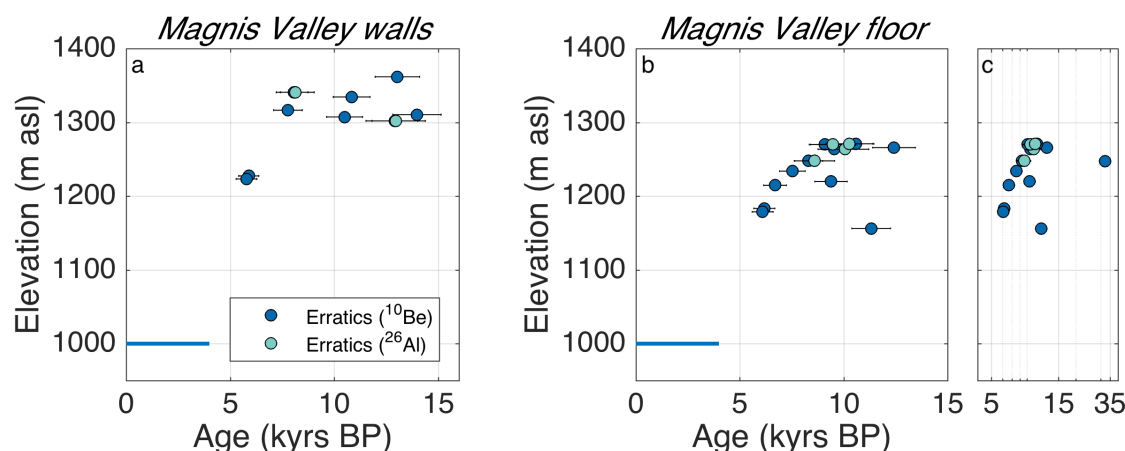
Two erratics from a recessional deposit on the upglacier valley wall record 120 m of glacier thinning by 5.8 kyr BP. Erratics on the valley floor largely agree with this history, showing 100 m of thinning by 6.1 kyr BP. Two of the erratics on the valley floor evidently have had prior exposure to cosmic rays (14-HAT-045-MV and 14-HAT-059-MV). Based on the lack of dated

erratics close to the ice margin, we are unable to determine the time at which the glacier margin stabilized at its present position

260 in Magnis Valley. However, if thinning continued at the same rate of ~5 cm/yr, the glacier would have established its modern margin position ~2 kyr BP, which is in agreement with the time at which the glacier margin stabilized at Lake Wellman.

Figure 4: Simplified map and sample locations at Magnis Valley. Blue curves indicated the mapped Britannia I (LGM) limit.
265 Ages corresponding to these samples are shown in Figure 5. Contours and satellite imagery from Land Information New Zealand (LINZ, 2010). Inset imagery from Bindschadler et al. (2008).

Figure 5: Magnis Valley exposure ages from the valley walls (**a**) and valley floor (**b**). Hatherton Glacier reached its limit in Magnis Valley ~13 kyr BP and began to retreat 7-8 kyr BP. Horizontal blue line shows elevation of present-day glacier margin. Panel **c** shows ages on a log scale in order to show samples with prior exposure to cosmic rays.

2.2.3 Lake Wellman

The exposure age chronology at Lake Wellman suffers from numerous pre-exposed erratics, resulting in a wide spread of ages (King et al., 2020; Storey et al., 2010) (). However, radiocarbon ages of algae from lakes and ponds show a strong dependence of age on elevation, with a maximum position at 9.5 kyr BP, followed by steady thinning to modern elevations by the late Holocene (King et al., 2020).
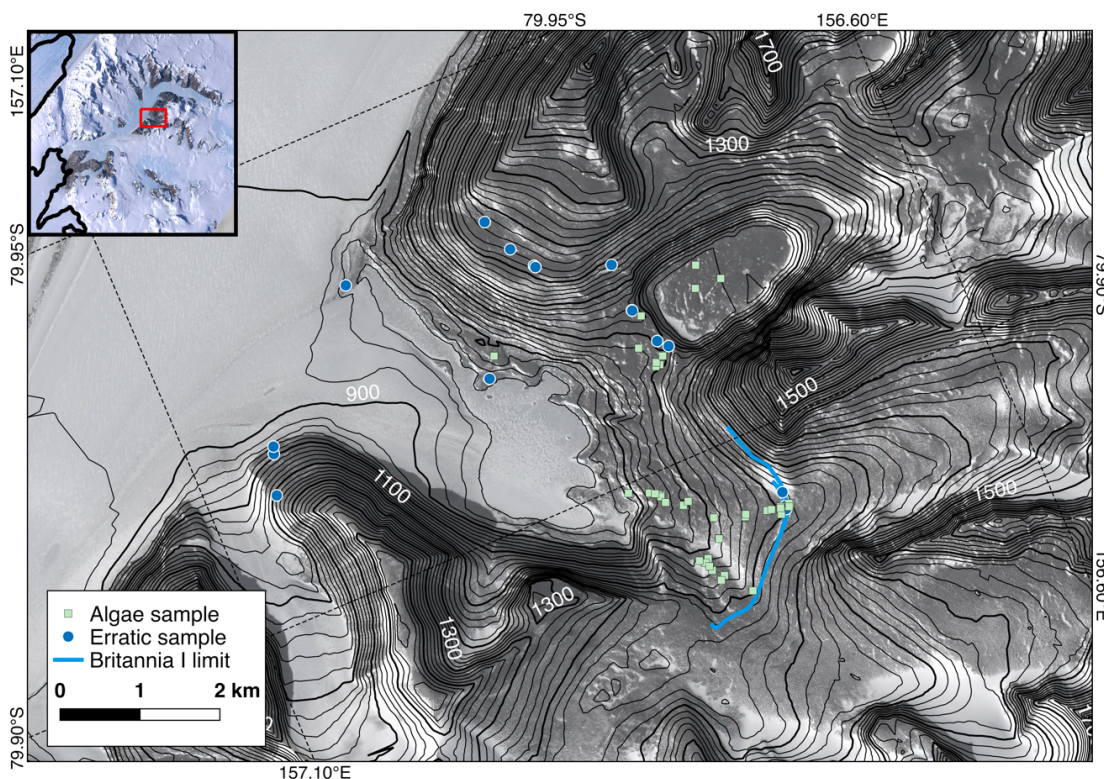
Figure 6: Simplified map of Lake Wellman and sample locations from King et al. (2020). Contours and satellite imagery from Land Information New Zealand (LINZ, 2010). Inset imagery from Bindschadler et al. (2008).

2.2.4 Brown Hills and Diamond Glacier

The Brown Hills lie north of Diamond Hill adjacent to Diamond Glacier—a distributary lobe of Darwin Glacier—and are bordered by the Ross Ice Shelf to the east (Figure 8). During glacial periods, Diamond Glacier would likely have crossed the Brown Hills and connected with the Ross Ice Sheet. Exposure ages of five erratics from the Brown Hills range from 7–205 kyr BP (Figure 9). Despite sampling the freshest, differentially-weathered erratics available, four of these ages are older than the maximum advance at sites on Hatherton Glacier, and they are not ordered by elevation or distance from the Diamond Glacier tongue. We interpret these samples as previously exposed erratics deposited by ice receding from its last maximum position, though it is also possible that they are undisturbed remnants of one or more older deposits. The youngest date from the Brown Hills also may be affected by inherited [10]Be, so we can only conclude that ice retreated from the saddle separating Diamond Glacier from the Ross Ice Sheet no earlier than 7 kyr BP.
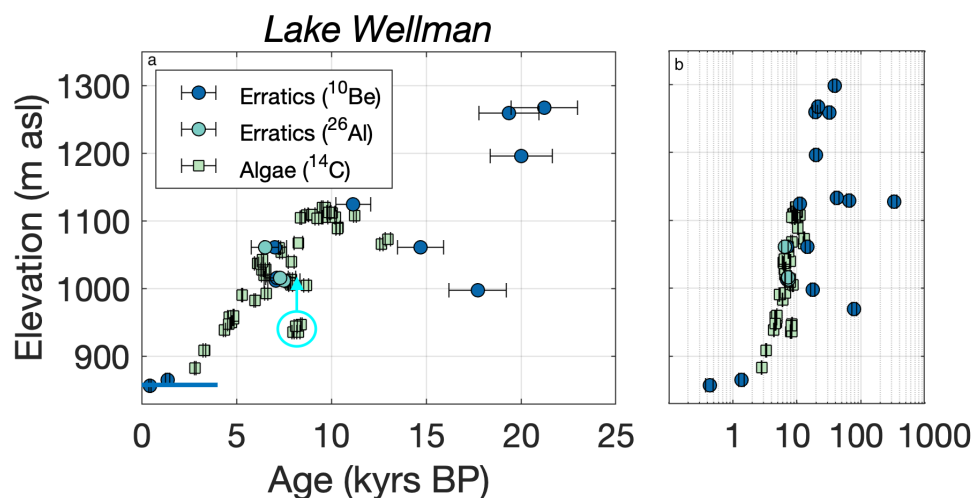
13

Figure 7: **a** Surface exposure ages and algae radiocarbon ages at Lake Wellman after King et al. (2020). Cyan arrow indicates elevation of sill that would have had to be overridden by ice to create the pond that hosted the samples in the cyan circle. Horizontal blue line shows elevation of present-day glacier margin. **b** All ages are shown on a logarithmic scale, in order to include a significant number of erratics with prior exposure to cosmic rays.

2.2.5 Diamond Hill

At Diamond Hill, at the mouth of Darwin Glacier, deposits are sparse and cannot be correlated with the drift succession described above. On the south slope of the mountain, above Darwin Glacier, fresh glacially-worked erratics are scattered over polished and striated bedrock outcrops. These clasts, stranded by the final stages of recession of Darwin Glacier, extend up to ~ 135 m above its present-day surface. Above this, bedrock becomes significantly more weathered and surfaces are largely devoid of transported boulders and cobbles. The geomorphic transition from surfaces shaped by wet-based glaciation at low altitude to heavily weathered upper slopes resembles transects on other peaks in the TAMs and Marie Byrd Land (e.g. Sugden et al., 2005). We attribute the geomorphic transition to differential erosion during the LGM and earlier glaciations. Ice in contact with the low-elevation bedrock was warm-based and erosive, but graded into thinner, cold-based ice cover at higher altitudes. A similar geomorphic gradient occurs in the Brown Hills and on the north slope of Diamond Hill, though bedrock is everywhere more weathered and there are very few lightly weathered erratics. Till deposits conceal much of the floor of the valley north of Diamond Hill, and fill the cirque below and west of the summit at ~800 m. Exhumation of lightly weathered clasts from these deposits may be a source of erratics with inherited nuclides in this area.
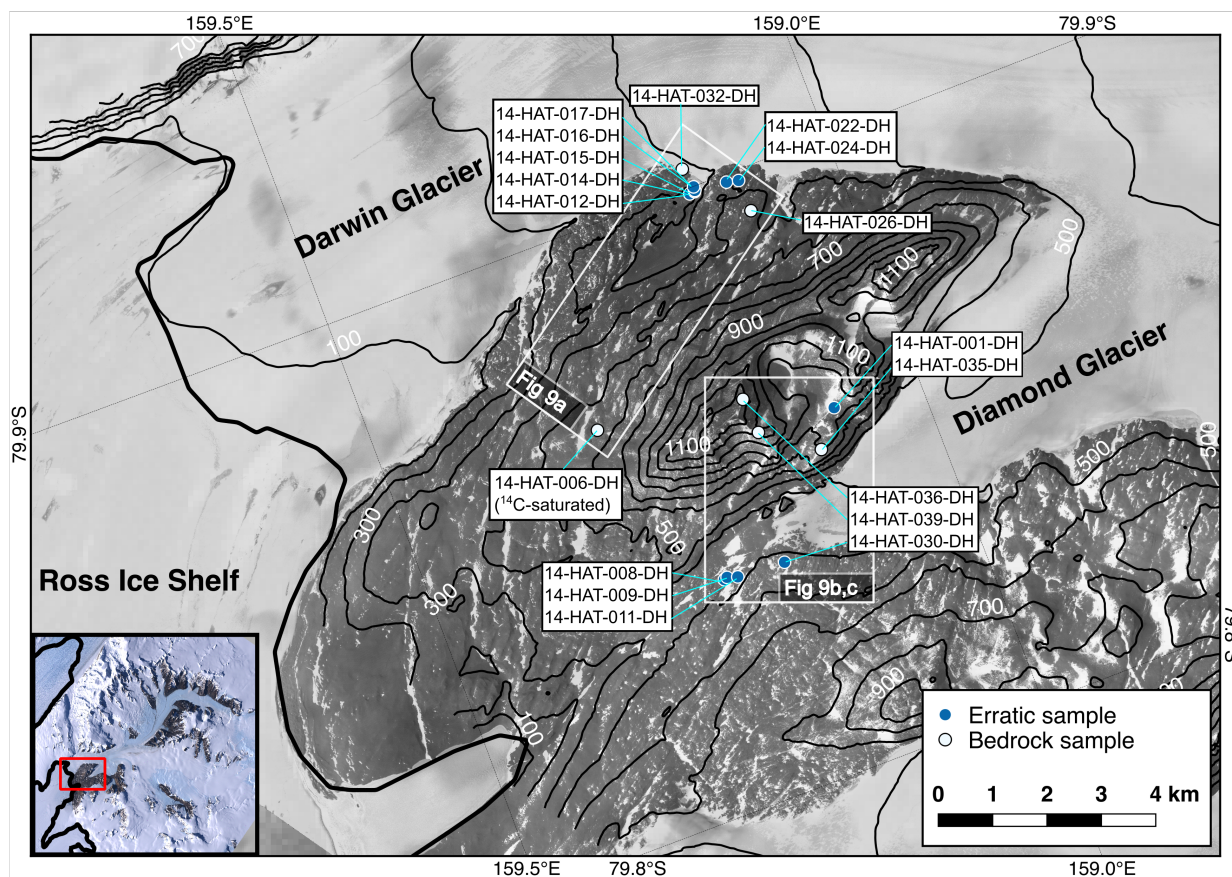
14

Figure 8: Map of Diamond Hill with bedrock and erratics sample locations. The modern grounding-line is shown as bold black line. Boxes indicate how samples are grouped into the panels of Figure 9. Sample numbers are included because of the complexity of the topography and exposure age distribution relative to the sample locations in previous figures. Contours and satellite imagery from Land Information New Zealand (LINZ, 2010). Inset imagery from Bindschadler et al. (2008). Missing elevation contours in the lower left corner of the map reflect the edge of the LINZ DEM.

The only relatively fresh, unweathered erratics that we found on Diamond Hill were perched on glacially sculpted bedrock domes overlooking Darwin Glacier, ~10 km upglacier from the modern grounding-line (Figure 8). There was no clear limit of deposition, but we did not find any relatively unweathered erratics higher than 135 m above the modern glacier margin. We analyzed eight of these erratics (Figure 9), which yield ^{10}Be ages spanning the latter half of the Holocene, from 5.2 ± 0.2 kyr BP at 135 m above the current glacier margin, to 0.3 ± 0.03 kyr BP at the current glacier margin. The rate of thinning matches the record from sub-fossil algae ^{14}C dates at Lake Wellman (King et al., 2020) (Figure 7), corroborating our inference that Hatherton Drift represents the last stages of the glacier's recession, separated from the youngest Britannia-I deposits by no

15

The Cryosphere
Discussions

Open Access

EGU

more than a few hundred years of still-stand or readvance. Thinning during these final stages appears to have been relatively constant between 5.2 and 3.1 kyr BP, after which it slowed.
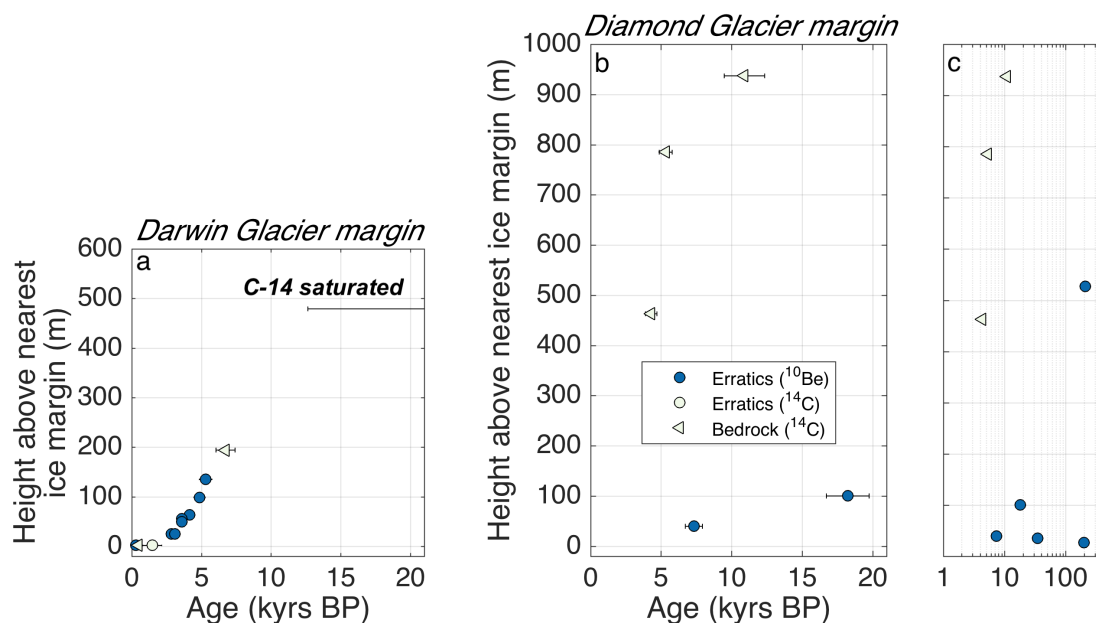

Figure 9: Diamond Hill chronology from *in-situ* [10]Be and ^{14}C exposure dating. Spatial distribution shown by white boxes in Figure 8. **a** Exposure ages from the side of Diamond Hill adjacent to Darwin Glacier. **b** Exposure ages from the Brown Hills and side of Diamond Hill (including summit samples) closer to Diamond Glacier. **c** All samples adjacent to Diamond Glacier on a logarithmic scale to show outliers. Bedrock ^{14}C ages give a maximum time of last exposure, because inherited ^{14}C from exposure before the LGM cannot be quantified. The top of Diamond Hill, >900 m above the modern glacier surface, was covered during the LGM and was exposed sometime after 11 kyr BP. In contrast, the ^{14}C-saturated sample ~500 m above present-day Darwin Glacier suggests more modest thickening at the LGM relative to present. Therefore, it is not straightforward to interpret these data without a glacier flow model, and not all ages can conceivably represent the glacier surface.

The lack of fresh deposits above 400 m on Diamond Hill does not necessarily imply ice-free conditions during the last glaciation. Based on the preservation of heavily weathered bedrock we presume that ice above this elevation was cold-based and debris-free, and thus did not deposit erratics as it retreated. Steep terrain and the extent of Diamond Hill prevented us from examining all locations, but we climbed to the summit of the mountain via the east (ice-shelf proximal) ridge, and descended on the northern (Brown Hills proximal) side, and we did not find evidence of a glacial maximum lateral moraine or recessional deposits above 400 m. Given both potential burial of surfaces by cold-based ice and the lack of erratics that would be suitable

for dating with [10]Be, we measured *in-situ*-produced ^{14}C in bedrock to determine the maximum thickening and retreat history of Darwin Glacier at its downstream end at Diamond Hill.

On the slopes of Diamond Hill immediately above Darwin Glacier, our highest bedrock sample (14-HAT-026-DH; 472 m a.s.l.) gives an apparent ^{14}C exposure age of 6.7 ± 0.7 kyr BP, extending the retreat history from [10]Be data to 200 m above the

350 modern glacier margin (Figure 9). Similarly, bedrock sampled <2 m above the current ice margin (14-HAT-033-DH; 280 m a.s.l.), and adjacent to the 300-year-old ([10]Be age) erratic (14-HAT-032-DH) gives an apparent ^{14}C exposure age of 500 ± 200 years BP. These ages confirm and extend the thinning chronology given by the [10]Be exposure ages. The exposure ages in this transect are too young to record, but do not preclude, a large early-Holocene deglaciation event, as found at Beardmore (Spector et al., 2017) and Mackay glaciers (Jones et al., 2015). However, those glaciers only thinned by tens of meters near the glacier

355 mouth following a large drawdown of several hundred meters in the early Holocene, whereas Darwin Glacier thinned by 200 m since 6.7 kyr BP, a history more similar to that at Reedy Glacier (Todd et al., 2010). The contrasting thinning histories may be a result of the ice sheet bed topography near the mouths of these glaciers, which is currently poorly known.

About 500 m above the glacier margin (593 m a.s.l.) on the east ridge of Diamond Hill, the bedrock is at or near saturation concentration with respect to in situ ^{14}C production-decay systematics (14-HAT-006-DH). This sample was either not covered

360 by ice during the last glaciation or was covered for only a brief period (< ~2 kyr). The maximum ice thickness at other locations in the Ross Sea lasted for 3-5 kyr (Todd et al., 2010; Hall et al., 2010; Spector et al., 2017), so this sample may be an upper bound on LGM ice surface elevation near the modern grounding line. This is a surprising result, given that the LGM ice surface was ~700-900 m above the modern ice surface at the mouths of other TAM outlet glaciers (Todd et al., 2010; Bromley et al., 2010, 2012; Spector et al., 2017), and 600-700 m above the modern ice shelf at Minna Bluff and on Ross Island (Anderson et

365 al., 2017; Denton and Marchant, 2000). It is at odds with both Bockheim et al.'s (1989) extrapolated LGM ice surface 1000 m above present at the mouth of Darwin Glacier, and with Storey et al.'s (2010) assertion that Darwin Glacier did not thicken during the LGM. Anderson et al.'s (2004) estimate of an LGM ice surface 800 m above the modern is closer to our potential LGM surface, but still appears to be an overestimate.

In contrast, on the summit and north flank of Diamond Hill — above Diamond Glacier — *in situ* [14]C concentrations are

370 well below saturation. Apparent exposure ages decrease with elevation from 10.8 ± 1.4 kyr at the summit of Diamond Hill (1287 m a.s.l.) to 5.3 ± 0.5 kyr at 1134 m a.s.l. and 4.3 ± 0.4 kyr at 813 m a.s.l. (Figure 9b). In contrast to the ages from the Darwin Glacier side of Diamond Hill, these ages suggest that the summit was covered by ice or snow for a long period during the last glaciation. Today, Diamond Glacier terminates in a bedrock saddle between Diamond Hill and the Brown Hills below these samples at ~350 m a.s.l. While Darwin Glacier had thinned to within 135 m of its modern thickness by ~5.1 kyr BP,

375 these ages seem to suggest that ice north of Diamond Hill was still at least 785 m thicker than present at this time, which is not glaciologically plausible.

We hypothesize that the ^{14}C-saturated sample (14-HAT-006-DH; 598 m a.s.l.) and the other samples near Darwin Glacier on the south side of Diamond Hill (Figure 9a) are more representative of large-scale ice fluctuations than the undersaturated samples from higher elevations on Diamond Hill (Figure 9b,c) for three reasons: (i) there is no evidence of glacial erosion

380   during the last glacial cycle for the high elevation samples, and therefore there are no mechanisms for producing older cosmogenic ^{14}C ages at low elevation than at high elevation, except for local ice or snow cover at those higher elevations; (ii) two of the three highest-elevation cosmogenic ^{14}C ages on Diamond Hill are younger than the bedrock and erratics ages nearest Darwin Glacier, which cannot be explained if all samples are interpreted to represent changes of the large-scale glacier surface; (iii) the summit of Diamond Hill (1287 m a.s.l.) is higher than the local LGM deposits reported by King et al. (2020) at Lake

385   Wellman (1130 – 1270 m a.s.l.; Figure 6; Figure 7), ~50 km upglacier. This interpretation implies that the exposure ages higher on Diamond Hill are the result of the disappearance of local ice or snow fields. However, given the limited number of in-situ ^{14}C exposure ages at Diamond Hill, these results are equivocal.

2.2.6 Summary of geochronologic constraints

We have presented geochronological data that constrain ice thickness along a flowline from near the head of Hatherton Glacier

390   to near the modern Darwin Glacier grounding line, based on: (i) [10]Be and [26]Al exposure ages of deposits from Bibra, Dubris and Magnis Valleys, (ii) radiocarbon dates of algae and [10]Be and [26]Al exposure ages from Lake Wellman (King et al., 2020), and (iii) [10]Be ages of erratics and *in-situ* [14]C exposure ages of bedrock from the south side of Diamond Hill adjacent to Darwin Glacier. Collectively these data suggest glacier advance and/or fluctuations at close to maximum thickness from ~14–8 kyr BP. At Lake Wellman, Magnis Valley, and Bibra/Dubris Valleys ice was at its maximum limit at 9.5 kyr BP, a time when

395   large outlet glaciers in the southern TAM were thinning at their mouths (Todd et al., 2010; Spector et al., 2017), and the grounding line of the Ross Sea Ice Sheet was retreating southwards (Hall et al., 2013; Goehring et al., 2019b). Dates of maximum thickness are not demonstrably different between the three sites on Hatherton Glacier, which also differs from the diachronous behavior of upper and middle Reedy Glacier (Todd et al., 2010), although the sizes of these glaciers and the distance between sites are very different. Our data from Diamond Hill show that Darwin Glacier thinned steadily by 200 m

400   since 6.7 kyr BP. However, the data are equivocal about the magnitude and rate of ice thickness changes near the grounding line in the early- to mid-Holocene. Data from nearest Darwin Glacier on Diamond Hill suggest slow and steady thinning of ~500 m through the Holocene, while data at the summit and north side of Diamond Hill suggest ~900 m of rapid thinning in the early-to-mid Holocene. We prefer the former interpretation, but we do not have enough data to rule out the latter. To examine these aspects of the glaciers' history and evolution we use a flowband model to simulate how these deglaciation

405   scenarios at the mouth of Darwin Glacier would be reflected in the chronologies from upstream on Hatherton Glacier. We also test the alternative hypothesis that 500 m of LGM-to-present thinning included a rapid drawdown in the early Holocene, consistent with records from other TAM outlet glaciers (e.g. Jones et al., 2015; Spector et al., 2017), followed by slow and steady thinning recorded in the ages of the erratics. These simulations are presented in the following section.

3 Numerical modelling of glacier fluctuations

410 ### 3.1 Model description

We modeled Darwin and Hatherton Glaciers since the LGM using a 1.5-D shallow ice glacier flowband model to evaluate possible deglaciation scenarios consistent with our geochronological data. Applying a simple ice-flow model to constrain ice-flow conditions and deglaciation behavior has been done for other TAM outlets (e.g., Anderson et al., 2004; Golledge et al., 2014; Jones et al., 2016). The model we apply solves the mass conservation equation to calculate ice thickness evolution using

415 the finite volume method. This model is computationally inexpensive and reduces the number of poorly constrained ice-flow parameters and boundary conditions. The model domain starts near Diamond Hill at 10 km upstream from the modern grounding-line where we have geochronological data. We do not model grounding-line evolution, but we are able to use geochronological data to prescribe surface-elevation change at a location that is always upstream of the grounding line over the past 20 kyr. This avoids the use of the shallow ice approximation near the grounding line, where the inherent assumptions in the model do not apply. We are thus able to use data to constrain aspects of the model that would otherwise require more

420 complexity, but where a more complex model would introduce additional parameters that are poorly known or completely unknown.

Ice flow in a flowband (1.5-D) is described by the time-evolving mass conservation equation (Cuffey and Paterson, 2010):

$$\frac{\partial H(x,t)}{\partial t} = -\frac{1}{W(x)}\left(\frac{\partial q(x,t)}{\partial x}\right) + \dot{b}(x,t) \tag{1}$$

where H(x,t) is the ice thickness, q(x,t) is the volumetric ice flux, W(x) is the glacier width, and $\dot{b}(x,t)$ is the surface mass

425 balance. Mass balance effects of melting or freezing at the glacier bed are neglected due to a lack of data. The total ice velocity (U) is the sum of contributions from internal deformation (U_d) and basal sliding (U_s) taken to be of this form:

$$U = U_d + U_S = f_d H \tau_d^n + f_s \frac{\tau_b^m}{H} \tag{2}$$

where f_d is the deformation factor, f_s is the sliding factor, n=3 is the flow-law exponent, $1/3 \le m \le 4$ is the sliding exponent, τ_d is the driving stress, and τ_b is the basal shear stress. Cross-sectional area is accounted for at each grid point. The modern fluxes from small tributary glaciers contributing to Darwin and Hatherton Glaciers are estimated using a flux gate calculation and we

430 make the assumption that these tributary flux contributions are constant through time.

3.2 Model parameters, tuning, and boundary conditions

Surface mass balance and basal conditions of Darwin and Hatherton glaciers are poorly known. We use the RACMO2.1 5.5-km resolution model of the modern surface mass balance (Lenaerts et al., 2012a), as this is the only data product to include the significant surface ablation that is observed. While these ablation areas do not occur in the same locations observed from

435 satellite imagery, we argue that this is the best choice of surface mass balance because it matches reasonably well the overall flux out of the glacier system (Gillespie et al., 2017). Furthermore, the model is a function of the integral of the surface mass

balance and not the specific pattern of accumulation and ablation at any given location. We also use the RACMO2.3 (van Wessem et al., 2014) 27-km resolution product along with scaling factors to simulate feasible LGM SMB scenarios. The two width-averaged RACMO SMB inputs and bed topography profiles (Gillespie et al., 2017) used for Hatherton and Darwin
440 glaciers shown in the Supplemental Material (Figures S1 and S2).

We tune a steady-state version of the flowband model to estimate poorly constrained ice-flow parameter values by minimizing the mismatch between the modeled and observed modern glacier surface elevation and the modern surface velocity at each model grid point. This strategy has been applied in related problems (e.g., Golledge et al., 2014). We vary the basal sliding factor (f_s) and the ice-flow deformation factor (f_d) defined at each model grid point within a plausible range of values.
445 The deformation factor and basal sliding parameter vary spatially over the model grid but we assume that the spatial patterns that optimize the fit to modern data have not changed over the past 20 kyr because there is not enough information available to constrain a different choice for the parameter values in the past. In general, we have limited information available to constrain the values of the sliding and deformation factors, and while our inferred patterns of these parameters generate a surface-elevation profile and surface-velocity profile that match modern values within their uncertainties, it is likely that it is not a
450 unique solution. However, we are using this simple model to constrain the time evolution of the glacier system that is consistent with our geochronological observations, and not to interpret inferred parameter values and patterns of controls on ice flow.

The downstream boundary condition for Darwin Glacier is a prescribed surface elevation through time based on our glacial geologic data. The surface elevation at the downstream boundary of the major tributary Hatherton Glacier is prescribed at each timestep by the value at the adjacent node along the Darwin Glacier flowline where the glaciers intersect, similar to what was
455 done by Anderson et al. (2004). At each timestep, the flux from Hatherton Glacier is added to Darwin Glacier at that node, the surface of Darwin Glacier is recalculated, and the surface elevation at the mouth of Hatherton Glacier is reset to match the updated surface of Darwin Glacier. While the model domains are set up to contain the modern drainages of Darwin and Hatherton Glaciers, these catchment boundaries may have changed in the past. Thus, we evaluate the influence of time-varying flux that enters the domain from the upstream boundary, as required by a flux-balance calculation. We are also able to modulate
460 flux entering the glacier through the upstream boundary as a way of investigating the role of catchment geometry changes (including ice divide migration) on the evolution of the glacier profiles.

3.3 Model evaluation

In order to compare the model output with our chronologies from each location, we must account for the fact that our geochronology data record the elevation of the glacier margin through time, rather than the glacier centerline that is calculated
465 in the flowband model. Thus, the exposure and radiocarbon ages represent a minimum elevation for the glacier centerline through time. While the glacier centerline generally lies 100 m above its margin today alongside our study sites, this would not necessarily have been the case at the LGM. We can determine the possible range of glacier centerline elevations at the LGM by calculating a linear best-fit curve to the LGM deposits in the valley floor (far from the modern glacier) and on the valley walls (close to the modern glacier). By extrapolating this linear fit out to the center of the glacier, we obtain a maximum

470   constraint on the LGM glacier centerline elevation because the glacier should not have a concave-up profile in the transverse direction. We use the elevation of the highest LGM erratics as a minimum constraint because the glacier margin can never be higher than the centerline. In the absence of further constraints, we use the mean of these elevations as the estimated LGM centerline elevation, and the span as the 2-sigma uncertainty. Because the age of the LGM deposit on the valley walls does not necessarily match the age of the corresponding limit on the valley floor, these are slightly time-transgressive estimates.

475   However, we consider this the best estimate possible without the use of a higher-dimensional glacier model that requires additional assumptions. We obtain glacier centerline elevations and 2-sigma uncertainties of 1355 ± 67 m at Lake Wellman, 1402 ± 56 m at Magnis Valley, and 1550 ± 45 m at Dubris-Bibra Valleys. Elevations from recessional deposits were then projected to estimate the centerline elevation by determining the percentage of total thinning each sample elevation represents and multiplying this by the height of the LGM surface above the modern glacier elevation. Model results are compared against

480   these projected elevations in Figure 10, Figure 11, and Figure 12.

      At Diamond Hill, we lack the clear limit of LGM deposits necessary to project samples to a glacier centerline elevation. Instead, we convert the elevations of bedrock and glacial erratics samples to a height above the nearest ice margin and use those values as constraints for glacier fluctuations and for the experiments discussed in Section 3.4. Likewise, we do not have a reliable means of assigning uncertainty to these glacier centerline elevations, which may be large. However, this uncertainty

485   is greatly outweighed by the uncertainty in what samples represent the elevation of Darwin Glacier versus local snow and ice fields.

3.4 Transient Experiments

Inputs for all experiments in this section are summarized in Table 1.

3.4.1 Experiment 1: 500 m of gradual thinning at the mouth of Darwin Glacier

490   *Modern surface mass balance, constant catchment size*

      Since we have no constraint on changes in accumulation and ablation patterns through time for the DHGS, we first set up a transient run in which the modern surface mass balance pattern is kept constant in time. The glacier surface at the outlet of Darwin Glacier is held at 500 m above the modern surface until 9 kyr BP to match the onset of thinning at Hatherton Glacier, and then lowered according to the geochronologic constraints from Diamond Hill (Figure 9), using the assumption that the

495   ^{14}C-saturated bedrock sample represents an upper bound on the LGM ice surface of the main trunk of Darwin Glacier. This is based on the interpretation that the Holocene ^{14}C exposure ages higher up on Diamond Hill represent cover by local ice or snow fields. The results of this experiment are shown in Figure 10 (DH_run_1a).

500

Table 1: Inputs for flowband model runs

Run code	Modern SMB	LGM SMB	External Flux Darwin (m³/yr)	External Flux Hatherton (m³/yr)
DH_run_1a	RACMO2.1	RACMO2.1	0	0
DH_run_1b	RACMO2.1	60% RACMO2.3	0	0
DH_run_1c	RACMO2.1	RACMO2.3	0	0
DH_run_1d	RACMO2.1	200% RACMO2.3	0	0
DH_run_1l	RACMO2.1	60% RACMO2.3	1.2×10^8	6.4×10^7
DH_run_2a	RACMO2.1	RACMO2.1	0	0
DH_run_2b	RACMO2.1	60% RACMO2.3	0	0
DH_run_2c	RACMO2.1	RACMO2.3	0	0
DH_run_2d	RACMO2.1	200% RACMO2.3	0	0
DH_run_2l	RACMO2.1	60% RACMO2.3	1.2×10^8	6.4×10^7
DH_run_3a	RACMO2.1	RACMO2.1	0	0
DH_run_3c	RACMO2.1	60% RACMO2.1	0	0
DH_run_3i	RACMO2.1	44% RACMO2.1 (scaled to Taylor Dome record)	-1.4×10^8	0

There is essentially no lag time between the application of the elevation-change at the mouth of Darwin and the response
505 of Hatherton Glacier in this scenario. Thus, the onset of thinning at each location along the profile of Hatherton Glacier occurs
almost simultaneously with the onset of thinning at Diamond Hill. This is consistent with our chronologies from the valleys
alongside Hatherton Glacier, each of which indicates that retreat began ~8-9 kyr BP. However, using the modern surface mass
balance at the LGM leads to a thinner modeled Hatherton Glacier than is indicated by the glacial deposits. This discrepancy is
more pronounced further upglacier: at Lake Wellman (close to the confluence of Darwin and Hatherton), the model predicts
510 an LGM ice surface ~75 m below the LGM erratics at the entrance to the valley; at Magnis Valley, the model underpredicts
LGM thickness by ~100 m; at Dubris and Bibra Valleys, the modeled glacier is ~170 m too thin.
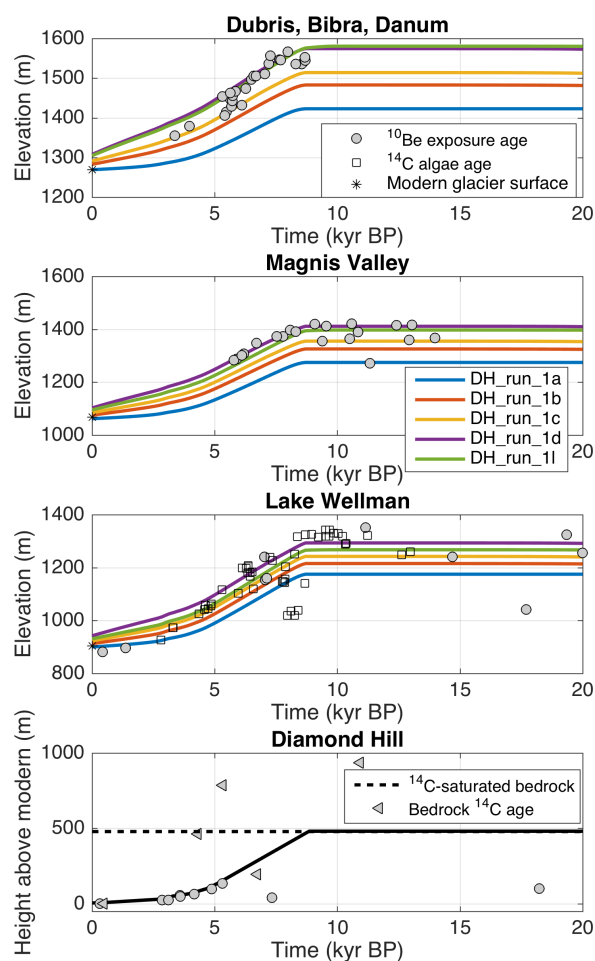
Figure 10: Flow-band model results from Experiment 1 compared with surface exposure ages from this study and surface exposure and radiocarbon ages from King et al. (2020), which have been projected to centerline elevations using the method described in Section 3.3. The two best-fitting scenarios require either a larger catchment for both glaciers at the LGM (green curve; DH_run_1l), or an accumulation rate far higher than modern (purple curve; DH_run_1d). The black curve in the Diamond Hill panel represents the prescribed ice surface history at the downstream boundary.

There are three possible explanations for the underprediction of LGM ice thickness in this experiment. First, it is possible that the current size of the glacier catchments is smaller than it was during the LGM. Observations of striated bedrock near the head of Hatherton Glacier indicate that at some unknown time in the past, ice likely flowed over into the Hatherton valley from what is now the catchment of Byrd Glacier (Bockheim et al., 1989). Likewise, there are no constraints on the former size of

23

the Darwin Glacier catchment. It is thus possible that more ice fed into the DHGS due to larger catchment size during the LGM. Second, our assumption of a constant pattern of surface mass balance through time is too simple. The large ablation areas found on both glaciers today are likely near their maximum extent, and a small climate perturbation would decrease their size, leading to a more positive surface mass balance (Brown and Scambos, 2004). However, Hatherton Glacier must have had ablation areas (both wind scouring and surface melt) at its margins during the local LGM in order to provide the meltwater necessary to create the ponds that hosted algae, and in order to deposit erratics in the valleys. Furthermore, accumulation rates tend to increase as the atmosphere warms during a glacial termination; the Taylor Dome ice core record shows a roughly 100% increase in accumulation rate between 12 kyr BP and 0.7 kyr BP (Monnin et al., 2004). The presence of blue ice areas due to scouring by katabatic winds would likely lead to a more complicated change in surface mass balance, but the reduction in snow accumulation during glacial periods would likely have been a common feature throughout the Transantarctic Mountains. Third, our records at the mouth of Darwin Glacier (Figure 9) are equivocal as discussed above. The fact that the complicated and spatially sparse bedrock ^{14}C record is difficult to interpret leaves open the possibility that the average LGM ice thickness at Diamond Hill was higher than we have tentatively concluded. We explore the effects of time-evolving surface mass balance, variable flux into the glacier canyons, and different LGM ice thickness at the mouth of Darwin Glacier in the following model experiments.

Time-evolving surface mass balance

We first examined the effect of scaling the modern surface mass balance to the normalized accumulation rate history recorded in the Taylor Dome ice core (Steig et al., 2000; Monnin et al., 2004). As expected, this also leads to a modeled Hatherton Glacier that is too thin at the LGM, with 150-250 m of thickening relative to modern. This gives a very poor fit to all of our glacial geologic data.

Next, we used a simpler time-varying surface mass balance pattern in an attempt to determine the magnitude of glacial-interglacial change needed to match the records from Hatherton Glacier using only variations in SMB. The modern surface mass balance is taken from RACMO 2.3. We defined the LGM surface mass balance by multiplying the RACMO 2.3 surface mass balance — which does not include ablation areas — by a scaling factor. We use values of 60%, 100%, and 200%. The choice of 60% is made to match the accumulation rate change in the Vostok ice core between the LGM and present (Petit et al., 1999). This is of course a crude estimation, but it results in reasonable LGM accumulation rates of 2-10 cm/yr. The surface mass balance is varied linearly in time between the modern and LGM states. After a 5 kyr spin-up to allow the model to equilibrate with LGM climate, the LGM SMB is held constant until 15 kyr, and then varied linearly to the modern SMB.

In this scenario, 60% scaling leads to underprediction of LGM ice thickness by about 100 m at all three Hatherton Glacier sites (DH_run_1b in Figure 10). Using a 200% scaling of RACMO2.3 SMB at the LGM leads to excellent agreement between the glacier model and most of the records from Hatherton Glacier (DH_run_1d in Figure 10). LGM surface elevations are matched to within a few tens of meters at all three locations, the timing and rate of thinning agree very well, and the modern surface elevations are reproduced to within 40 m at all three locations.

24

While the 200% scaling results in a reasonable match between the model and surface-exposure age data, it produces an unlikely surface mass balance history. This requires LGM accumulation rates of 7-30 cm/yr, compared to ~3 cm/yr accumulation at Taylor Dome during the same time period. The fact that at least some surface ablation had to occur to create

560 ice-marginal ponds means total surface mass balance may have been even lower than at Taylor Dome. This scenario also requires the overall surface mass balance to decrease during the termination of the glacial period, which is unlikely. Although this scenario fits our data quite well, we search for a more reasonable explanation.

Added flux to account for changing catchment area

565 As noted above, there are no constraints on the size of the glacier catchments at the LGM. While the modern glacier catchments are kept small by their proximity to Byrd and Mulock Glaciers, they could have been larger at the LGM. Due to the low surface slopes of the EAIS and the small size of the DHGS catchment relative to those of Byrd and Mulock Glaciers, just a moderate amount of localized thickening or thinning could drastically increase or decrease the drainage area contributing to Darwin and Hatherton. To account for this uncertainty, we take the simple approach of adding ice flux to the upstream

570 boundary of the Darwin and Hatherton Glacier model domains. A challenge of this approach is to define a time series of flux change across the upstream boundaries. Because this value would have varied in time and would not necessarily have been the same for both glaciers, any solution is likely to be non-unique. However, the goal of this exercise is not to calculate the magnitude of the flux entering the glaciers at the LGM, but rather to determine whether changing catchment areas could be a reasonable means of achieving the LGM ice thickness of Hatherton Glacier.

575 When additional flux is added only to Hatherton Glacier, the glacier profile tends to steepen, leading to overprediction of ice thickness by >100 m at Dubris-Bibra and Magnis valleys, while ice thickness is still ~75 m too low at Lake Wellman. Conversely, when a proportional amount of flux is added to the upstream boundary of the Darwin Glacier domain, LGM ice thickness is underpredicted at all locations on Hatherton Glacier by 75-100 m, while the head of Darwin Glacier is ~200 m thicker than Bockheim et al. (1989) found at Darwin Nunatak. However, by adding a more modest amount of flux to both

580 Darwin and Hatherton Glaciers, and by using the scaled SMB of 60% modern for the LGM, we achieve a better fit to the LGM limits and retreat histories at all three locations along Hatherton Glacier, without unduly thickening the head of Darwin Glacier (DH_run_1l in Figure 10). Given the uncertainties in bed properties, accumulation rate, and tributary fluxes through time we consider this to be a satisfactory fit to the data. If the catchment boundaries stabilized before the grounding line of Darwin Glacier stopped retreating, this could also explain the slowdown of thinning at Dubris-Bibra Valleys several kyr prior to the

585 slowdown of thinning at Lake Wellman, ~30 km closer to the grounding line.

We now consider whether the amount of additional incoming flux required to match the LGM limits is a physically reasonable quantity. For the additional 6.4×10^7 m^3/yr added to Hatherton and the additional 1.2×10^8 m^3/yr added to Darwin and a reasonable LGM accumulation rate of 3 cm/yr over the East Antarctic Plateau, this would require 2,100 km^2 and 4,100 km^2 of additional LGM catchment area for Hatherton and Darwin glaciers, respectively. This represents a ~75% increase over

590 the modern catchment area (Gillespie et al., 2017), but only a 5% decrease in the Mulock Glacier catchment or a 0.5% decrease
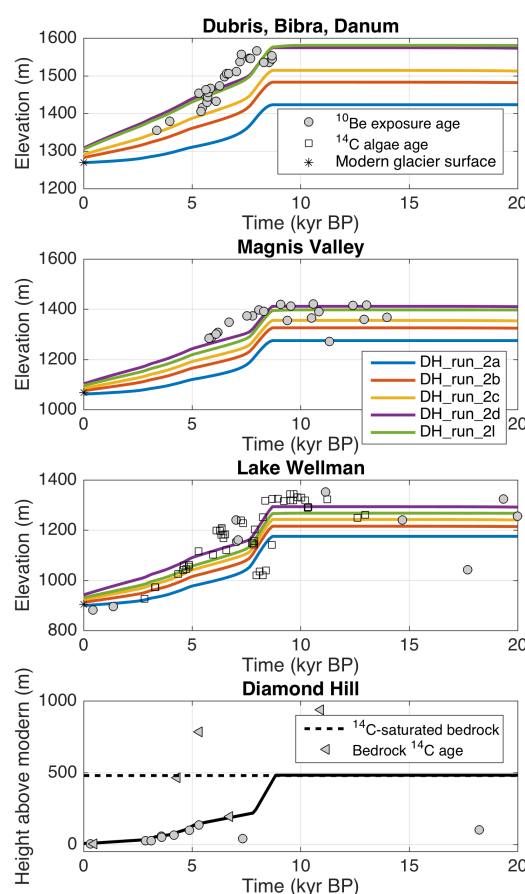
in the Byrd Glacier catchment areas based on values calculated by Stearns (2011). Because this total areal change is roughly equivalent to the reported uncertainty in the Mulock Glacier catchment area, and only about 11% of the uncertainty in the Byrd Glacier catchment area, we consider this amount of divide migration over a glacial-interglacial cycle to be reasonable.

3.4.2 Experiment 2: Rapid early-Holocene thinning at the mouth of Darwin Glacier

595   This experiment, like Experiment 1, assumes the ^{14}C-saturated bedrock at Diamond Hill represents the upper limit of the LGM ice surface. Other records from the western Ross Embayment show a rapid drawdown event 9-8 kyr BP, presumably indicating widespread deglaciation of the region in the early Holocene (Spector et al., 2017). There is no record of such abrupt thinning at Hatherton Glacier, but such an event could have occurred in the data gap between the ^{14}C-saturated and the 6.7 kyr bedrock (separated by 300 m of elevation) at the mouth of Darwin Glacier. We explore this possibility by imposing a rapid

600   thinning event of 275 m (similar to thinning at Beardmore and Mackay glaciers (Jones et al., 2015; Spector et al., 2017)) from 9-8 kyr BP, followed by gradual thinning consistent with the glacial geologic constraints. Surface mass balance and additional flux are the same as the best-fit scenario from Experiment 1 (i.e., 75% larger catchment, SMB varies linearly through time). The results of this experiment are shown Figure 11.

The rapid thinning imposed at the mouth of Darwin Glacier propagates upglacier in the model with no significant lag.

605   While the amplitude of the signal decays with distance upglacier, it is still readily detectable in the modeled glacier changes at Dubris-Bibra Valleys. This leads to a much poorer fit to the data than the situation with gradual thinning at the Darwin Glacier mouth in Experiment 1. This shows that the records from Hatherton Glacier are not consistent with an episode of rapid thinning at the mouth of Darwin Glacier, which implies that the DHGS did not respond to the last deglaciation in the same way as other outlet glaciers to the north and south (e.g., Jones et al., 2015; Spector et al., 2017).

610

Figure 11: Flow-band model results for Experiment 2. All inputs are the same as for Experiment 1, except for the downstream boundary condition, which contains a period of rapid deglaciation 9-8 kyr BP. It is evident that this event would have been recorded in the deposits at Hatherton Glacier, but there is no clear evidence of this in our chronologies. Thus, the case of slow thinning in Experiment 1 provides a better fit to the data.

615

3.4.3 Experiment 3: 950 m of thinning at the mouth of Darwin Glacier, with a rapid pulse of thinning in the mid-Holocene

This experiment, unlike Experiments 1 and 2, assumes the ^{14}C-saturated bedrock at Diamond Hill is merely an outlier, and that the exposure ages at higher elevations represent the fluctuations of Darwin Glacier. While we have argued that the higher-elevation ages are not as representative of the surface of Darwin Glacier as they are of more local ice configuration, we do not have enough data to prove this assertion. Thus, in this experiment we evaluate a scenario in which Darwin Glacier was 1 km

620

thicker than present at the LGM and covered the top of Diamond Hill, after which it thinned by ~800 m from 6-4 kyr BP. This thinning history is defined by the bedrock samples in Figure 9b. Results are shown in Figure 12.
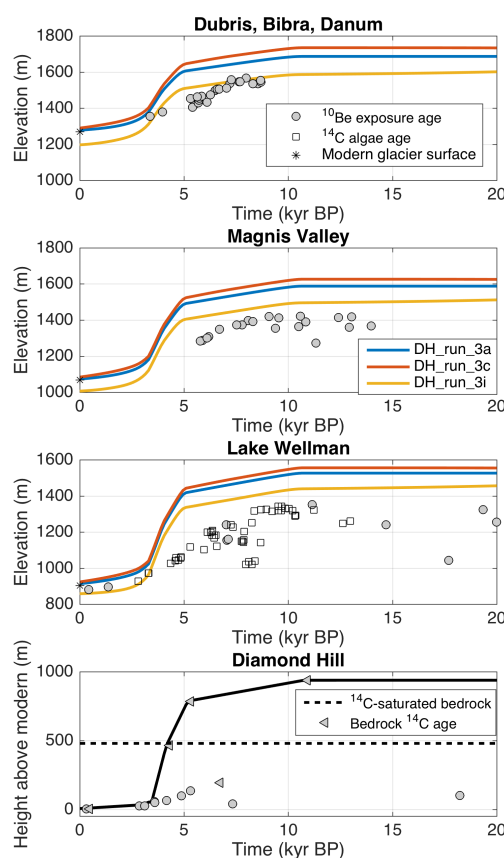

Figure 12: Flow-band model results for Experiment 3, in which we assume that the Holocene exposure ages high on Diamond Hill represent thinning of the main trunk of Darwin Glacier. Fitting the LGM thickness of Hatherton Glacier requires a much smaller Darwin Glacier catchment at the LGM, but we cannot fit the shape of the chronologies with any combination of simple assumptions about surface mass balance or catchment area. Thus, we rule out this scenario as unlikely and conclude that the young exposure ages at high elevation on Diamond Hill may reflect more local ice fluctuations.

For RACMO2.1 accumulation rates and modern catchment boundaries, this deglaciation scenario leads to a modeled Hatherton Glacier that is ~160 – 200 m too thick at all locations on Hatherton Glacier (DH_run_3a in Figure 12). Scaling the RACMO2.1 accumulation rate to the Taylor Dome record, which is our lowest LGM accumulation rate, produces essentially no change in the glacier profiles, while scaling the RACMO 2.3 SMB by 60% leads to a worse fit due to the lack of ablation

28

635   zones (DH_run_3c in Figure 12). The fit to Hatherton Glacier LGM ice thickness can be improved by moving the Darwin

Glacier catchment boundary ~25 km into the model domain (i.e., decreasing the catchment area; DH_run_3i in Figure 12).

There is no geologic evidence for this, but it may not be an unreasonable amount of change, given the enormous catchment

areas of Byrd and Mulock glaciers. However, the rapid thinning during deglaciation propagates upglacier in all three model

runs, leading to a very poor fit to the records of Hatherton Glacier fluctuations. Thus, the pattern of thinning cannot be matched

640   using simple assumptions about catchment size or surface mass balance, and thus we conclude that this is an unlikely scenario.

This supports our earlier hypothesis that the elevation transect near the modern margin of Darwin Glacier at Diamond Hill

(Figure 9a) most closely represents the major ice thickness fluctuations since the LGM, while the chronology from the Brown

Hills and high on Diamond Hill represent more local ice or snowfield fluctuations (Figure 9b,c).

4 Ice sheet model ensemble

645   Our flowband model is only applied to the grounded portions of Darwin and Hatherton Glaciers, and thus cannot be used

to directly examine the effect of grounding-line retreat on the ice thickness of Darwin and Hatherton glaciers. To investigate

regional controls we use the Pennsylvania State University 3-D ice sheet model (PSUICE) (e.g., Pollard and DeConto, 2012a)

to examine the LGM-to-present retreat of Byrd, Darwin-Hatherton, and Mulock glaciers. PSUICE uses a combination of the

shallow ice and shallow shelf approximations (SIA and SSA, respectively) along with a parameterization of grounding-line

650   flux (Schoof, 2007) to allow for full continent-scale simulations on kyr to Myr timescales, as well as an optimized model-

parameter set that is tuned to match glacial geologic data from around West Antarctica over the past 20 kyr (Pollard et al.,

2016). However, because we are only interested here in the ice sheet in the Ross Sea, this parameter set tuned at the continent

scale may not be the most suitable for our regional investigation. So, we setup an ensemble of model runs to investigate the

sensitivity to the choice of key parameter values. First, we run the model at 20-km resolution over the whole continent from

655   25 ka to present, and use this to establish boundary conditions for an ensemble of 48 nested model simulations at 10 km

resolution since 20 ka in which we vary model parameters around the values optimized from Pollard et al. (2016). While this

resolution may not be sufficient to accurately represent the dynamics of Darwin and Hatherton glaciers, we use these model

runs to investigate regional deglaciation. The modern ice discharge from those glaciers (~0.2 Gt/yr at present; Gillespie et al.,

2017) is small compared to that from Byrd and Mulock glaciers (~27.5 Gt/yr at present; Stearns, 2011), so DHGS does not

660   affect large-scale and long-time evolution of the Ross Sea Ice Sheet. We are interested in the relationship between ice thickness

at the TAM front and the position of the Ross Ice Sheet grounding-line, and thus do not need to model the individual glaciers

at high resolution. The 10-km resolution was chosen as a trade-off between computing time and the ability to resolve pinning

points that may have a large effect on grounding-line evolution. We vary four model parameters that were examined by Pollard

et al. (2016): basal traction on the modern seafloor, isostatic rebound rate, ice shelf melt sensitivity to ocean temperatures, and

665   a calving rate factor. We also use two different sea-level curves to explore the dependence of the model on time resolution in

proxy records (Lisiecki and Raymo, 2005; Spratt and Lisiecki, 2016). Parameter values used in the ensemble are listed in Table

2. Because our results show more gradual and recent deglaciation of the DHGS than at other locations in the TAM (Spector et al., 2017), our choice of parameter values is intended to slow down grounding-line retreat relative to the optimized parameter set of Pollard et al. (2016).

670

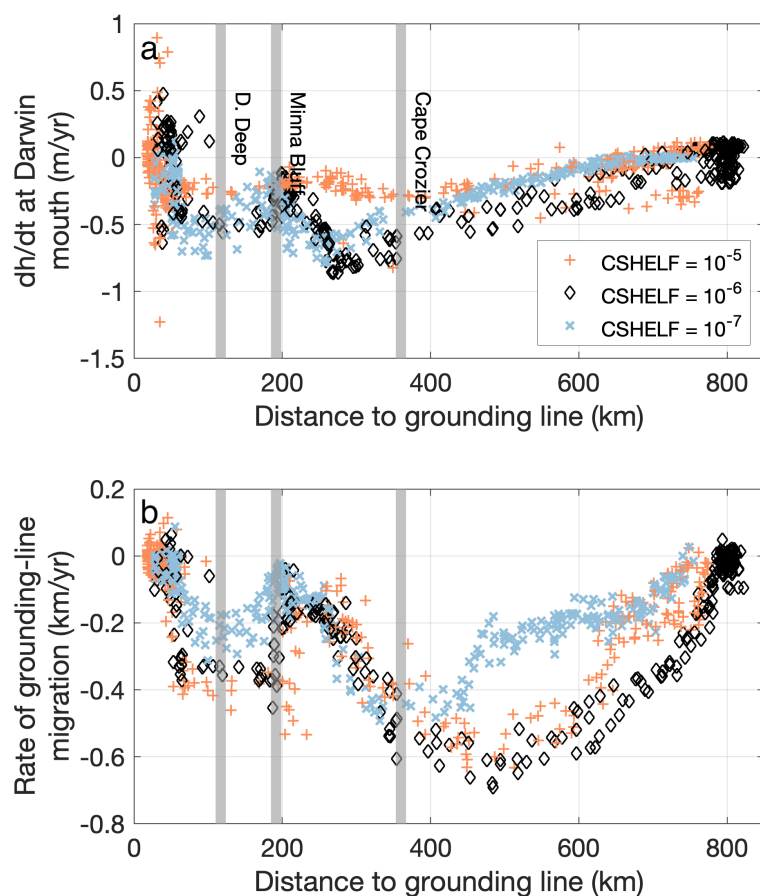Table 2: Parameter choices for ice sheet model ensemble

Parameter	Values	Optimal value from Pollard et al. (2016)
Asthenospheric rebound timescale	1000, 2000 yrs	2000 yrs
Sub-shelf melting factor	0.5, 1	1, 3
Basal sliding coefficient on seafloor	10^{-5}, 10^{-6}, 10^{-7}	10^{-5}
Calving factor	0.7, 1	1
Sea-level curve	Lisiecki and Raymo, 2005; Spratt and Lisiecki, 2016	Only used Lisiecki and Raymo, 2005

We investigate the relationship between rates of grounding-line retreat and ice thickness change at the mouth of Darwin Glacier. Ideally, we seek a combination of model parameters that enable the grounding line to slowly approach the mouth of 675 Darwin Glacier, despite the steeply back-sloping bed topography south of Minna Bluff, while still leading to early Holocene deglaciation of much of the western Ross Embayment (Spector et al., 2017). However, we also recognize that the parameters could vary in space and time, so this solution could be non-unique. Furthermore, higher-order ice physics and adaptive mesh refinement to resolve grounding-line evolution may be required to fully capture the processes involved in the retreat but require too much computational expense to be included in an ensemble of model runs over timescales of tens of thousands of years.

680 Results from our ice sheet model ensemble are shown in Figure 13. We find that no combination of the parameters we explored reproduces the slow and steady drawdown through the Holocene that we observe in the glacial geologic data at Diamond Hill or at other locations along Hatherton Glacier. The basal sliding coefficient leads to a difference of ~600 m ice thickness between the fastest sliding value (10^{-5}) and the slowest (10^{-7}). While the ice at the mouth of Darwin Glacier begins thinning ~1 kyr earlier for the faster sliding scenarios, modern ice thickness is achieved by 5-6 kyr BP in all model runs, which 685 is much earlier than our glacial chronologies show (~2-3 kyr BP). While none of the model runs in this ensemble achieve what we consider to be a good fit to our data from Diamond Hill, the three clusters of model runs defined by the three basal sliding coefficients display internally consistent behavior characteristics that are worth examining in order to better understand the sensitivity of the Ross Sea Ice Sheet near the mouth of Darwin Glacier.

690

Figure 13: Results from the 48-member PSUICE ice-sheet model ensemble. **a** The relationship between rate of ice thickness change at the mouth of Darwin Glacier and the distance to the grounding-line for all ice sheet model runs. The basal sliding parameter (CSHELF) has by far the largest effect of the parameters we explored in the ensemble. Grey bars indicate the locations of the features we hypothesized to affect the rate of grounding-line retreat: Cape Crozier, Minna Bluff, and the

695 Discovery Deep. **b** Grounding-line migration rate as a function of distance to the grounding line from Darwin Glacier. Negative values indicate retreat. Migration rate slows after the ice around Cape Crozier goes afloat, but thinning rates at Darwin Glacier remain relatively constant or increase. Ice thinning at the mouth of Darwin Glacier accelerates significantly in all model runs after the grounding line has retreated past Minna Bluff, indicating that this feature provided a stabilizing backpressure to the grounded Ross Sea Ice Sheet. Perhaps counterintuitively, the acceleration of grounding-line retreat into the back-sloping

700 Discovery Deep is not always accompanied by increased thinning rates at the mouth of Darwin Glacier. This indicates that there might not be a large thinning signal in glacial deposits near the mouth of Darwin Glacier, even for a very rapid pulse of grounding-line retreat.

The Cryosphere
Discussions
Open Access

EGU

After an initial spin-up period during which the modeled ice sheet reaches a quasi-equilibrium thickness, each group of
705   model runs shows a complex relationship between rates of thickness changes near Darwin Glacier and the rate of grounding-
line retreat. All three groups of model runs undergo slow, almost linear thinning as the grounding line retreats from its LGM
position to Cape Crozier. Once the grounding-line is upstream of Cape Crozier, the model behavior diverges based on the basal
sliding parameter: while all runs see a drastic decreasing in the rate of grounding-line retreat, the runs with the largest sliding
value exhibit a slower rate of thinning at Darwin Glacier, while thinning rate in the runs with lower sliding values continues
710   to accelerate before it suddenly slows. Once the grounding line retreats behind Minna Bluff, grounding-line retreat and thinning
at Darwin Glacier accelerates in all runs; however, the largest acceleration in grounding-line retreat corresponds to the lowest
response in thinning rates at Darwin Glacier. The acceleration of the grounding-line as it retreats into Discovery Deep is not
generally reflected in thinning rates at Darwin Glacier. This suggests that some pulses of rapid grounding-line retreat may not
have left a strong signal of thinning at the mouth Darwin Glacier, and this may have possibly occurred at other TAM outlet
715   glaciers. Given the complex relationship the model predicts between ice thinning rates at the mouth of Darwin Glacier and the
rate of grounding-line retreat, we refrain from interpreting our glacier chronologies in terms of the rate of grounding-line
retreat. However, it is still valid to interpret the cessation of major changes in glacier thickness ~3 kyr BP as a sign that the
grounding line had reached close to its modern position at the mouth of Darwin Glacier.

5 Discussion

720   Darwin and Hatherton glaciers continued to adjust to regional deglaciation until ~3 kyr BP, which means that the grounding
line likely did not arrive at its present location until about that time. Darwin and Hatherton Glaciers lie roughly halfway
between McMurdo Sound and Beardmore Glacier, which both deglaciated in the early Holocene (Hall et al., 2004; Spector et
al., 2017), yet the timing of grounding-line arrival at Darwin Glacier is apparently much more recent. This could imply that a
large region extending across Byrd, Darwin, and Mulock glaciers remained grounded for about 4 kyr after the grounding-line
725   in the central Ross Embayment had retreated further south. It remains an open question how far along the TAM front this
grounded ice persisted, and if it comprised a single, grounded ice mass or local piedmont lobes (Lee et al., 2017).

It is unclear if the chronology from Skelton Glacier supports this interpretation, as there are no erratics near the grounding
line that date to the last deglaciation (Jones et al., 2017). A small number of erratics at locations far from the modern grounding
line suggest that most thinning in the Skelton Névé had occurred by 6 kyr BP (Jones et al., 2017; Anderson et al., 2020), but
730   the number of samples is too small to determine the rate of thinning or the timing of its onset. More data from Skelton Glacier
are needed for thorough comparison with the chronology at Darwin and Hatherton glacier.

Steady thinning of Hatherton Glacier through the Holocene supports a later arrival of the grounding line relative to glaciers
to the north and south (Hall et al., 2015; Jones et al., 2015; Spector et al., 2017). In our flowband model, thinning at the mouth
of Darwin Glacier propagates rapidly upglacier; thus, the deposits alongside Hatherton Glacier can be interpreted as recording

735   the relative rates of ice thinning at the mouth of Darwin Glacier. There is no record of an exceptionally fast period of thinning at Hatherton Glacier, in agreement with our interpretation of the sparse data near the modern grounding line. However, our ice sheet model ensemble analysis suggests that periods of exceptionally fast grounding-line retreat — such as across the Discovery Deep region — would not necessarily correspond to noticeably faster ice thinning rates at the mouth of Darwin Glacier. A two- to four-fold increase in the modeled rate of grounding-line retreat as ice in Discovery Deep goes afloat does

740   not cause faster drawdown at Darwin Glacier for most of the parameter values we investigated. In the scenarios with the fastest basal sliding, there is an increase in the rate of thinning when the grounding-line retreats into Discovery Deep. However, this lags the change in the grounding-line retreat rate and reaches a maximum thinning rate after the grounding line has already slowed. This suggests that the time at which the grounding-line arrived at the glacier mouth may be deducible from geologic data, but that there are significant complications in drawing conclusions about relative rates of grounding-line retreat from

745   glacier-elevation proxies.

        While we are not able to determine the rate of grounding-line retreat, we can make a first-order estimate of the sensitivity of Darwin and Hatherton glaciers to grounding-line position using records from elsewhere in the Ross Sea. The grounding-line retreated past Ross Island >8.6 kyr BP (McKay et al., 2016), and McMurdo Sound became free of grounded ice between 7.5 and 9 kyr BP (Hall et al., 2004; Jones et al., 2015; Anderson et al., 2017; Christ and Bierman, 2020). This is similar to the

750   time at which Hatherton Glacier began to retreat from its last high-stand (8 – 9 kyr BP), and our glacier modeling suggests Darwin likely began thinning around this same time as well. Thus, Darwin and Hatherton glaciers may be strongly dependent on the ice configuration near Ross Island. The results of our ice sheet model ensemble suggest that this relationship is complex, as different parameter choices lead to opposing behavior as the grounding-line retreat past Cape Crozier. This discrepancy should be addressed with further modeling studies of outlet glacier response to grounding-line retreat and/or more data from

755   near the modern grounding line of Darwin Glacier. The more rapid thinning of Mackay and Beardmore glaciers could be due to the steeply back-sloping bed topography in the immediate vicinity of the glacier mouths (Jones et al., 2015; Spector et al., 2017).

        Our estimated LGM ice surface elevation of ~600 m asl at the mouth of Darwin Glacier from our flowband modeling needs to be reconciled with the elevations of the LGM limit of 637 m asl at Minna Bluff (Denton and Marchant, 2000) and 520 m

760   asl at Mt. Discovery (Anderson et al., 2017). The flowband of Darwin Glacier likely would have passed between these sites at the LGM (Denton and Hughes, 2000), and with our inferred ice surface elevation the glacier surface profile would have been very flat at the LGM, resulting in lower driving stresses than we would expect in comparison to modern glaciers and ice streams (c.f. Cuffey and Paterson, 2010, pg 297). We identify three factors that could reconcile these elevation differences and lead to a sufficient LGM surface slope between Darwin Glacier and Minna Bluff-to-Mt. Discovery.

765   First, there is significant uncertainty in the large-scale ice surface elevation that corresponds to the ^{14}C-saturated bedrock elevation at Diamond Hill. Ablation by katabatic winds can cause large difference in surface elevations around a nunatak (Bintanja, 1999). The downglacier side of Diamond Hill may have been subject to especially vigorous wind-driven ablation at the LGM, and thus could have been significantly lower than the large-scale ice surface. As we have shown, the fit of our

flowband model results to the data at Hatherton Glacier is more sensitive to rates of thickness change at the glacier mouth than
770 to the absolute LGM ice thickness. Therefore, the possibility that the glacier centerline LGM ice surface could have been
significantly higher (perhaps ~100–200 m) than the ^{14}C-saturated bedrock sample at Diamond Hill is not in necessarily in
conflict with our preferred deglaciation scenario, as long as thinning was smooth, steady, and initiated around 9 kyr BP.

Second, none of the reported LGM surface elevations include the effects of glacial isostatic adjustment, which could vary
widely between Darwin Glacier and Minna Bluff. Geothermal flux south of Ross Island may be 58–125% higher than at
775 Diamond Hill (Morin et al., 2010; An et al., 2015). If the crustal densities around Minna Bluff and Ross Island are
correspondingly lower than at the mouth of Darwin Glacier, the loading of the crust by grounded ice would have caused greater
isostatic depression at Minna Bluff than at Darwin Glacier, potentially reconciling these elevation differences.

Third, the majority of the Ross Sea Drift on Minna Bluff is found significantly lower than the reported LGM maximum of
637 m asl reported by Denton and Marchant (2000). Only one small patch occurs higher than 500 m asl; this defines the
780 reported 637 m asl LGM limit (see Plate 1 in Christ and Bierman, 2020). As there are no numeric age constraints at this
location, it is possible that this represents a short-lived (~1 kyr) transient maximum that could have also occurred at Diamond
Hill, but would not be detectable by our *in-situ* [14]C measurement. The short-lived maximum at Lake Wellman reported by
King et al. (2020) supports this hypothesis.

Ice sheet model simulations of the last deglaciation — including the ensemble presented here, as well as those of Pollard
785 et al. (2016), Kingslake et al. (2018); Lowry et al. (2019, 2020); and Albrecht et al. (2020) — do not predict steady thinning
of the mouth of Darwin Glacier during the last deglaciation. These models all predict a rapid drawdown at the mouth of Darwin
Glacier around 10 kyr BP as the grounding-line retreats between Minna Bluff and the TAM front. The models generally agree
poorly with glacial geologic data in the McMurdo Sound region as well, causing it to deglaciate thousands of years earlier than
glacial geologic data suggest. This is not surprising, given that ice-sheet model sensitivity to climate forcing is strongly
790 sensitive to a number of poorly known parameters (Pollard et al., 2016; Lowry et al., 2020), climate forcing itself is poorly
known, and the Bedmap2 topography beneath the modern day Ross Ice Shelf used by these models is coarsely resolved
(Fretwell et al., 2013). Including new constraints on bed topography (Tinto et al., 2019; Morlighem et al., 2020) could lead to
different model behavior. Additionally, the large ensemble experiments that are tuned to glacial geologic data (Pollard et al.,
2016; Albrecht et al., 2020) attempt to fit data from around West Antarctica or the whole continent and thus might sacrifice
795 predictive skill in the Ross Embayment to improve the overall ensemble score when tuning spatially homogeneous parameter
values. Tuning parameters using a large ensemble over the Ross Embayment alone could lead to a better fit between models
and data.

We suggest that the relatively recent and slow deglaciation of the DHGS is likely due to the convergence of Byrd and
Mulock Glaciers near the mouth of Darwin Glacier and/or lateral drag past Minna Bluff and Cape Crozier, which would both
800 have led to dynamic ice thickening that opposed grounding-line retreat. Numerical investigations of grounding-line dynamics
have shown that convergent flow can counteract the acceleration of dynamic thinning as the grounding line retreats down a
reverse bed slope (Gudmundsson, 2013); positive strain rates measured south of Minna Bluff show that convergent flow and

compression are causing dynamic thickening of the ice shelf in this region today (Thomas et al., 1984). Whillans and Merry (2001) identified Cape Crozier and Minna Bluff as controlling obstacles to the flow of the modern Ross Ice Shelf, and we

805 expect they would have had a similar effect during the last deglaciation. Together, the effects of convergent flow and lateral drag could have created a protected embayment that resisted grounding-line retreat for longer than glaciers farther to the south, even given the steeply back-sloping bed topography of Discovery Deep. This lends support to the hypothesis that Byrd Glacier is of fundamental importance to the stability of ice in the Ross Sea sector (Hughes et al., 2017).

6 Conclusions

810 We have dated deposits of the DHGS in order to help constrain the timing and pattern of grounding-line retreat in the Ross Embayment since the Last Glacial Maximum. The data suggest a later and slower deglaciation than that experienced by glaciers both farther south (e.g. Spector et al., 2017) and farther north (Jones et al., 2015). The scarcity of glacial deposits near the modern grounding line of Darwin Glacier and absence of deposits immediately adjacent to the grounding line make it difficult to directly interpret the thickness and timing of the LGM at the mouth of Darwin Glacier. We used a 1.5-D glacier flowband

815 model to evaluate possible deglaciation scenarios for Darwin Glacier that are consistent with our new data and we used a 3-D ice sheet model to evaluate the sensitivity of model reconstructions of regional deglaciation to poorly known model parameters. Our key findings are:

• LGM glacial deposits in ice-free valleys alongside Hatherton Glacier record up to 450 m of thickening relative to present at Lake Wellman, 350 m at Magnis Valley, and 300 m at Dubris Valley. The glacier margin extended several kilometers into

820 each valley during its maximum before receding slowly and steadily through the Holocene. It did not reach its present thickness until ≤2.8 kyr BP.

• Erratics perched stably on granitic bedrock at Diamond Hill, which is 10 km upstream of the modern grounding-line, record 135 m of thinning of Darwin Glacier between 5.1 kyr BP and 300 yr BP, with most of that thinning complete by 3 kyr BP.

• Maximum bedrock ^{14}C exposure ages indicate two possible, but conflicting, thinning histories at the mouth of Darwin Glacier:

825 the LGM surface of Darwin Glacier was either >190m but <~500 m above the modern glacier and thinned steadily through the mid-Holocene, or it was ~950 m thicker than present with ~600–800 m of rapid thinning in the mid Holocene.

• We used a glacier flowband model to test the two conflicting deglaciation scenarios suggested by the data at the mouth of Darwin Glacier. Flowband model results show that our data are most consistent with ~500 m slow and steady thinning at the mouth of Darwin Glacier between ~9 kyr BP and ~3 kyr BP, accompanied by a large decrease in catchment area through the

830 Holocene. Rapid deglaciation at the glacier mouth — like that exhibited by other major glaciers in the Ross Embayment — is not consistent with our geochronologic data. The fit of the model results to the data from Hatherton Glacier is more sensitive to rates of ice thickness change than to the absolute LGM ice thickness.

• An ensemble of 48 runs using a 3-D ice-sheet model indicates that using glacial geologic data of ice-elevation change to constrain even relative rates of grounding-line retreat is not straightforward. Counter to expectation, periods of more rapid

The Cryosphere
Discussions

835 grounding-line migration may correspond to relatively constant thinning at outlet glacier mouths. The presence of pinning points such as Cape Crozier reduces the rate of modeled grounding-line retreat, but not necessarily the rate of thinning at Darwin Glacier. Thus, rates of thinning from glacial geologic records at Darwin and Hatherton glaciers should not be directly interpreted as reflecting rates of grounding-line retreat. This may also be true of other glaciers that we have not examined here.

• We suggest that the relatively slow thinning of Darwin and Hatherton Glaciers through the last deglaciation could be the
840 result of convergent flow of Darwin Glacier with Byrd, Mulock, and Skelton glaciers, along with lateral drag due to the flow past Minna Bluff.

850 *Author contributions:* TRH, JOS, BH, and CK conducted fieldwork and sample collection. TRH, JOS, and CK prepared and analyzed samples for ^{10}Be and ^{26}Al. KN and BG prepared and analyzed rock samples for ^{14}C. MRK and TRH developed the glacier flowband model code. MRK, TRH, and HC designed, performed, and analyzed glacier flowband model experiments. TRH designed, performed, and analyzed 3D ice sheet model experiments. MKG provided gridded ice thickness and bed topography product for the flowband model experiments. TRH wrote the manuscript with input from all authors.
855

Competing interests: The authors declare they have no conflict of interest.

Data and code availability: Cosmogenic isotope data are archived on the Informal Cosmogenic-Nuclide Exposure-Age Database at ice-d.org. Flowband model code is available at https://github.com/mkoutnik/DH_code. Penn State Ice Sheet model
860 code is not publicly available, as it is the intellectual property of David Pollard. Flowband and ice-sheet model output will be made available on the University of Washington ResearchWorks Archive.

References

Albrecht, T., Winkelmann, R. and Levermann, A.: Glacial-cycle simulations of the Antarctic Ice Sheet with the Parallel Ice Sheet Model (PISM) – Part 2: Parameter ensemble analysis, The Cryosphere, 14(2), 633–656, doi:10.5194/tc-14-633-2020,
865 2020.

An, M., Wiens, D. A., Zhao, Y., Feng, M., Nyblade, A., Kanao, M., Li, Y., Maggi, A. and Lévêque, J.-J.: Temperature, lithosphere-asthenosphere boundary, and heat flux beneath the Antarctic Plate inferred from seismic velocities, Journal of Geophysical Research: Solid Earth, 120(12), 8720–8742, doi:10.1002/2015JB011917, 2015.

Anderson, B. M., Hindmarsh, R. C. A. and Lawson, W. J.: A modelling study of the response of Hatherton Glacier to Ross Ice
870   Sheet grounding line retreat, Global and Planetary Change, 42(1–4), 143–153, doi:10.1016/j.gloplacha.2003.11.006, 2004.

Anderson, J. B., Conway, H., Bart, P. J., Witus, A. E., Greenwood, S. L., McKay, R. M., Hall, B. L., Ackert, R. P., Licht, K., Jakobsson, M. and Stone, J. O.: Ross Sea paleo-ice sheet drainage and deglacial history during and since the LGM, Quaternary Science Reviews, 100, 31–54, doi:10.1016/j.quascirev.2013.08.020, 2014.

Anderson, J. T. H., Wilson, G. S., Fink, D., Lilly, K., Levy, R. H. and Townsend, D.: Reconciling marine and terrestrial
875   evidence for post LGM ice sheet retreat in southern McMurdo Sound, Antarctica, Quaternary Science Reviews, 157, 1–13, doi:10.1016/j.quascirev.2016.12.007, 2017.

Anderson, J. T. H., Wilson, G. S., Jones, R. S., Fink, D. and Fujioka, T.: Ice surface lowering of Skelton Glacier, Transantarctic Mountains, since the Last Glacial Maximum: Implications for retreat of grounded ice in the western Ross Sea, Quaternary Science Reviews, 237, 106305, doi:10.1016/j.quascirev.2020.106305, 2020.

880   Balco, G., Todd, C., Huybers, K., Campbell, S., Vermeulen, M., Hegland, M., Goehring, B. M. and Hillebrand, T. R.: Cosmogenic-nuclide exposure ages from the Pensacola Mountains adjacent to the Foundation Ice Stream, Antarctica, Am J Sci, 316(6), 542–577, doi:10.2475/06.2016.02, 2016.

Baroni, C. and Hall, B. L.: A new Holocene relative sea-level curve for Terra Nova Bay, Victoria Land, Antarctica, Journal of Quaternary Science, 19(4), 377–396, doi:10.1002/jqs.825, 2004.

885   Bindschadler, R., Vornberger, P., Fleming, A., Fox, A., Mullins, J., Binnie, D., Paulsen, S. J., Granneman, B. and Gorodetzky, D.: The Landsat Image Mosaic of Antarctica, Remote Sensing of Environment, 112(12), 4214–4226, doi:10.1016/j.rse.2008.07.006, 2008.

Bintanja, R.: On the glaciological, meteorological, and climatological significance of Antarctic blue ice areas, Rev. Geophys., 37(3), 337–359, doi:10.1029/1999RG900007, 1999.

890   Bockheim, J. G., Wilson, S. C., Denton, G. H., Andersen, B. G. and Stuiver, M.: Late Quaternary ice-surface fluctuations of Hatherton Glacier, Transantarctic Mountains, Quaternary Research, 31(2), 229–254, 1989.

Bromley, G. R. M., Hall, B. L., Stone, J. O., Conway, H. and Todd, C. E.: Late Cenozoic deposits at Reedy Glacier, Transantarctic Mountains: implications for former thickness of the West Antarctic Ice Sheet, Quaternary Science Reviews, 29(3–4), 384–398, doi:10.1016/j.quascirev.2009.07.001, 2010.

895   Bromley, G. R. M., Hall, B. L., Stone, J. O. and Conway, H.: Late Pleistocene evolution of Scott Glacier, southern Transantarctic Mountains: implications for the Antarctic contribution to deglacial sea level, Quaternary Science Reviews, 50, 1–13, doi:10.1016/j.quascirev.2012.06.010, 2012.

Brown, I. C. and Scambos, T. A.: Satellite monitoring of blue-ice extent near Byrd Glacier, Antarctica, Annals of Glaciology, 39(1), 223–230, doi:10.3189/172756404781813871, 2004.

900 Christ, A. J. and Bierman, P. R.: The local Last Glacial Maximum in McMurdo Sound, Antarctica: Implications for ice-sheet behavior in the Ross Sea Embayment, GSA Bulletin, 132(1–2), 31–47, doi:10.1130/B35139.1, 2020.

Conway, H.: Past and Future Grounding-Line Retreat of the West Antarctic Ice Sheet, Science, 286(5438), 280–283, doi:10.1126/science.286.5438.280, 1999.

Conway, H., Hall, B. L., Denton, G. H., Gades, A. M. and Waddington, E. D.: Past and Future Grounding-Line Retreat of the
905 West Antarctic Ice Sheet, Science, 286(5438), 280–283, doi:10.1126/science.286.5438.280, 1999.

Cuffey, K. M. and Paterson, W. S. B.: The physics of glaciers, Academic Press., 2010.

Denton, G. H. and Hughes, T. J.: Reconstruction of the Ross ice drainage system, Antarctica, at the last glacial maximum, Geografiska Annaler: Series A, Physical Geography, 82(2–3), 143–166, 2000.

Denton, G. H. and Marchant, D. R.: The geologic basis for a reconstruction of a grounded ice sheet in McMurdo Sound,
910 Antarctica, at the last glacial maximum, Geografiska Annaler: Series A, Physical Geography, 82(2–3), 167–211, 2000.

Denton, G. H., Bockheim, J. G., Wilson, S. C., Leide, J. E. and Andersen, B. G.: Late Quaternary ice-surface fluctuations of Beardmore Glacier, Transantarctic Mountains, Quaternary Research, 31(2), 183–209, doi:10.1016/0033-5894(89)90005-7, 1989.

Ditchburn, R. G. and Whitehead, N. E.: The separation of ^{10}Be from silicates, [online] Available from:
915 http://inis.iaea.org/Search/search.aspx?orig_q=RN:27007501 (Accessed 17 October 2017), 1994.

Dowdeswell, J. A., Ottesen, D., Evans, J., Cofaigh, C. Ó. and Anderson, J. B.: Submarine glacial landforms and rates of ice-stream collapse, Geology, 36(10), 819–822, doi:10.1130/G24808A.1, 2008.

Fretwell, P., Pritchard, H. D., Vaughan, D. G., Bamber, J. L., Barrand, N. E., Bell, R., Bianchi, C., Bingham, R. G., Blankenship, D. D., Casassa, G., Catania, G., Callens, D., Conway, H., Cook, A. J., Corr, H. F. J., Damaske, D., Damm,
920 V., Ferraccioli, F., Forsberg, R., Fujita, S., Gim, Y., Gogineni, P., Griggs, J. A., Hindmarsh, R. C. A., Holmlund, P., Holt, J. W., Jacobel, R. W., Jenkins, A., Jokat, W., Jordan, T., King, E. C., Kohler, J., Krabill, W., Riger-Kusk, M., Langley, K. A., Leitchenkov, G., Leuschen, C., Luyendyk, B. P., Matsuoka, K., Mouginot, J., Nitsche, F. O., Nogi, Y., Nost, O. A., Popov, S. V., Rignot, E., Rippin, D. M., Rivera, A., Roberts, J., Ross, N., Siegert, M. J., Smith, A. M., Steinhage, D., Studinger, M., Sun, B., Tinto, B. K., Welch, B. C., Wilson, D., Young, D. A., Xiangbin, C. and Zirizzotti, A.: Bedmap2:
925 improved ice bed, surface and thickness datasets for Antarctica, The Cryosphere, 7(1), 375–393, doi:10.5194/tc-7-375-2013, 2013.

Gillespie, M. K., Lawson, W., Rack, W., Anderson, B., Blankenship, D. D., Young, D. A. and Holt, J. W.: Geometry and ice dynamics of the Darwin–Hatherton glacial system, Transantarctic Mountains, Journal of Glaciology, 1–14, doi:10.1017/jog.2017.60, 2017.

930 Goehring, B. M., Wilson, J. and Nichols, K.: A fully automated system for the extraction of in situ cosmogenic carbon-14 in the Tulane University cosmogenic nuclide laboratory, Nuclear Instruments and Methods in Physics Research Section B: Beam Interactions with Materials and Atoms, doi:10.1016/j.nimb.2019.02.006, 2019a.

Goehring, B. M., Balco, G., Todd, C., Moening-Swanson, I. and Nichols, K.: Late-glacial grounding line retreat in the northern Ross Sea, Antarctica, Geology, doi:10.1130/G45413.1, 2019b.

935 Golledge, N. R., Marsh, O. J., Rack, W., Braaten, D. and Jones, R. S.: Basal conditions of two Transantarctic Mountains outlet glaciers from observation-constrained diagnostic modelling, Journal of Glaciology, 60(223), 855–866, doi:10.3189/2014JoG13J131, 2014.

Greene, C. A., Gwyther, D. E. and Blankenship, D. D.: Antarctic mapping tools for MATLAB, Computers & Geosciences, 104, 151–157, 2017.

940 Halberstadt, A. R. W., Simkins, L. M., Greenwood, S. L. and Anderson, J. B.: Past ice-sheet behaviour: retreat scenarios and changing controls in the Ross Sea, Antarctica, The Cryosphere, 10(3), 1003–1020, doi:10.5194/tc-10-1003-2016, 2016.

Hall, B. L., Baroni, C. and Denton, G. H.: Holocene relative sea-level history of the Southern Victoria Land Coast, Antarctica, Global and Planetary Change, 42(1), 241–263, doi:10.1016/j.gloplacha.2003.09.004, 2004.

Hall, B. L., Denton, G. H., Stone, J. O. and Conway, H.: History of the grounded ice sheet in the Ross Sea sector of Antarctica
945 during the Last Glacial Maximum and the last termination, Geological Society, London, Special Publications, 381(1), 167–181, doi:10.1144/SP381.5, 2013.

Hall, B. L., Denton, G. H., Heath, S. L., Jackson, M. S. and Koffman, T. N. B.: Accumulation and marine forcing of ice dynamics in the western Ross Sea during the last deglaciation, Nature Geoscience, 8(8), 625–628, doi:10.1038/ngeo2478, 2015.

950 Hendy, C. H.: Late Quaternary Lakes in the McMurdo Sound Region of Antarctica, Geografiska Annaler: Series A, Physical Geography, 82(2–3), 411–432, doi:10.1111/j.0435-3676.2000.00131.x, 2000.

Hughes, T., Zhao, Z., Hintz, R. and Fastook, J.: Instability of the Antarctic Ross Sea Embayment as climate warms, Rev. Geophys., 55(2), 2016RG000545, doi:10.1002/2016RG000545, 2017.

Jones, R. S., Mackintosh, A. N., Norton, K. P., Golledge, N. R., Fogwill, C. J., Kubik, P. W., Christl, M. and Greenwood, S.
955 L.: Rapid Holocene thinning of an East Antarctic outlet glacier driven by marine ice sheet instability, Nat Commun, 6, 8910, doi:10.1038/ncomms9910, 2015.

Jones, R. S., Norton, K. P., Mackintosh, A. N., Anderson, J. T. H., Kubik, P., Vockenhuber, C., Wittmann, H., Fink, D., Wilson, G. S., Golledge, N. R. and McKay, R.: Cosmogenic nuclides constrain surface fluctuations of an East Antarctic outlet glacier since the Pliocene, Earth and Planetary Science Letters, 480, 75–86, doi:10.1016/j.epsl.2017.09.014, 2017.

960 Joy, K., Fink, D., Storey, B. and Atkins, C.: A 2 million year glacial chronology of the Hatherton Glacier, Antarctica and implications for the size of the East Antarctic Ice Sheet at the Last Glacial Maximum, Quaternary Science Reviews, 83, 46–57, doi:10.1016/j.quascirev.2013.10.028, 2014.

King, C., Hall, B., Hillebrand, T. and Stone, J.: Delayed maximum and recession of an East Antarctic outlet glacier, Geology, 48(6), 5, 2020.

965 Kingslake, J., Ely, J. C., Das, I. and Bell, R. E.: Widespread movement of meltwater onto and across Antarctic ice shelves, Nature, 544(7650), 349–352, doi:10.1038/nature22049, 2017.

Kingslake, J., Scherer, R. P., Albrecht, T., Coenen, J., Powell, R. D., Reese, R., Stansell, N. D., Tulaczyk, S., Wearing, M. G. and Whitehouse, P. L.: Extensive retreat and re-advance of the West Antarctic Ice Sheet during the Holocene, Nature, 558(7710), 430–434, doi:10.1038/s41586-018-0208-x, 2018.

970 Kohl, C. P. and Nishiizumi, K.: Chemical isolation of quartz for measurement of in-situ-produced cosmogenic nuclides, Geochimica et Cosmochimica Acta, 56(9), 3583–3587, 1992.

Lee, J. I., McKay, R. M., Golledge, N. R., Yoon, H. I., Yoo, K.-C., Kim, H. J. and Hong, J. K.: Widespread persistence of expanded East Antarctic glaciers in the southwest Ross Sea during the last deglaciation, Geology, G38715.1, doi:10.1130/G38715.1, 2017.

975 Lenaerts, J. T., Van Den Broeke, M. R., Scarchilli, C. and Agosta, C.: Impact of model resolution on simulated wind, drifting snow and surface mass balance in Terre Adélie, East Antarctica, Journal of Glaciology, 58(211), 821–829, 2012.

LINZ: Antarctic topographic data, Land Information New Zealand (LINZ) [online] Available from: https://www.linz.govt.nz/data/linz-data/topographic-data/antarctic-topographic-data (Accessed 18 September 2019), 2010.

Lisiecki, L. E. and Raymo, M. E.: A Pliocene-Pleistocene stack of 57 globally distributed benthic δ18O records,
980 Paleoceanography, 20(1), PA1003, doi:10.1029/2004PA001071, 2005.

Lowry, D. P., Golledge, N. R., Bertler, N. A. N., Jones, R. S. and McKay, R.: Deglacial grounding-line retreat in the Ross Embayment, Antarctica, controlled by ocean and atmosphere forcing, SCIENCE ADVANCES, 13, 2019.

Lowry, D. P., Golledge, N. R., Bertler, N. A. N., Jones, R. S., McKay, R. and Stutz, J.: Geologic controls on ice sheet sensitivity to deglacial climate forcing in the Ross Embayment, Antarctica, Quaternary Science Advances, 1, 100002,
985 doi:10.1016/j.qsa.2020.100002, 2020.

Monnin, E., Steig, E. J., Siegenthaler, U., Kawamura, K., Schwander, J., Stauffer, B., Stocker, T. F., Morse, D. L., Barnola, J.-M., Bellier, B., Raynaud, D. and Fischer, H.: Evidence for substantial accumulation rate variability in Antarctica during the Holocene, through synchronization of CO2 in the Taylor Dome, Dome C and DML ice cores, Earth and Planetary Science Letters, 224(1–2), 45–54, doi:10.1016/j.epsl.2004.05.007, 2004.

990 Morin, R. H., Williams, T., Henrys, S. A., Magens, D., Niessen, F. and Hansaraj, D.: Heat Flow and Hydrologic Characteristics at the AND-1B borehole, ANDRILL McMurdo Ice Shelf Project, Antarctica, Geosphere, 6(4), 370–378, doi:10.1130/GES00512.1, 2010.

Morlighem, M., Rignot, E., Binder, T., Blankenship, D., Drews, R., Eagles, G., Eisen, O., Ferraccioli, F., Forsberg, R., Fretwell, P., Goel, V., Greenbaum, J. S., Gudmundsson, H., Guo, J., Helm, V., Hofstede, C., Howat, I., Humbert, A., Jokat,
995 W., Karlsson, N. B., Lee, W. S., Matsuoka, K., Millan, R., Mouginot, J., Paden, J., Pattyn, F., Roberts, J., Rosier, S., Ruppel, A., Seroussi, H., Smith, E. C., Steinhage, D., Sun, B., Broeke, M. R. van den, Ommen, T. D. van, Wessem, M. van and Young, D. A.: Deep glacial troughs and stabilizing ridges unveiled beneath the margins of the Antarctic ice sheet, Nature Geoscience, 13(2), 132–137, doi:10.1038/s41561-019-0510-8, 2020.

Nichols, K. A. and Goehring, B. M.: Isolation of quartz for cosmogenic in situ C-14 analysis, Geochronology, 1(1), 43–52,
1000 doi:10.5194/gchron-1-43-2019, 2019.

Noonan, B., Zawar-Reza, P. and Lawson, W.: Boundary-layer climate of the Darwin-Hatherton Glacial System, Antarctica: meso- and synoptic-scale circulations: Darwin-Hatherton Boundary-layer Climate, Antarctica, International Journal of Climatology, 35(12), 3608–3623, doi:10.1002/joc.4235, 2015.

Petit, J.-R., Jouzel, J., Raynaud, D., Barkov, N. I., Barnola, J.-M., Basile, I., Bender, M., Chappellaz, J., Davis, M., Delaygue, G. and others: Climate and atmospheric history of the past 420,000 years from the Vostok ice core, Antarctica, Nature, 399(6735), 429–436, 1999.

Pollard, D. and DeConto, R. M.: Modelling West Antarctic ice sheet growth and collapse through the past five million years, Nature, 458(7236), 329–332, doi:10.1038/nature07809, 2009.

Pollard, D. and DeConto, R. M.: Description of a hybrid ice sheet-shelf model, and application to Antarctica, Geosci. Model Dev., 5(5), 1273–1295, doi:10.5194/gmd-5-1273-2012, 2012.

Pollard, D., Chang, W., Haran, M., Applegate, P. and DeConto, R.: Large ensemble modeling of the last deglacial retreat of the West Antarctic Ice Sheet: comparison of simple and advanced statistical techniques, Geosci. Model Dev., 9(5), 1697–1723, doi:10.5194/gmd-9-1697-2016, 2016.

Rignot, E., Mouginot, J. and Scheuchl, B.: Ice flow of the Antarctic ice sheet, Science, 333(6048), 1427–1430, 2011.

Spector, P., Stone, J., Cowdery, S. G., Hall, B., Conway, H. and Bromley, G.: Rapid early-Holocene deglaciation in the Ross Sea, Antarctica, Geophys. Res. Lett., 2017GL074216, doi:10.1002/2017GL074216, 2017.

Spratt, R. M. and Lisiecki, L. E.: A Late Pleistocene sea level stack, Climate of the Past, 12(4), 1079–1092, doi:https://doi.org/10.5194/cp-12-1079-2016, 2016.

Stearns, L. A.: Dynamics and mass balance of four large East Antarctic outlet glaciers, Annals of Glaciology, 52(59), 116–126, 2011.

Steig, E. J., Morse, D. L., Waddington, E. D., Stuiver, M., Grootes, P. M., Mayewski, P. A., Twickler, M. S. and Whitlow, S. I.: Wisconsinan and Holocene Climate History from an Ice Core at Taylor Dome, Western Ross Embayment, Antarctica, Geografiska Annaler: Series A, Physical Geography, 82(2–3), 213–235, doi:10.1111/j.0435-3676.2000.00122.x, 2000.

Stone, J. O.: Air pressure and cosmogenic isotope production, J. Geophys. Res., 105(B10), 23753–23759, doi:10.1029/2000JB900181, 2000.

Storey, B. C., Fink, D., Hood, D., Joy, K., Shulmeister, J., Riger-Kusk, M. and Stevens, M. I.: Cosmogenic nuclide exposure age constraints on the glacial history of the Lake Wellman area, Darwin Mountains, Antarctica, Antarctic Science, 22(06), 603–618, doi:10.1017/S0954102010000799, 2010.

Sugden, D. E., Balco, G., Cowdery, S. G., Stone, J. O. and Sass, L. C.: Selective glacial erosion and weathering zones in the coastal mountains of Marie Byrd Land, Antarctica, Geomorphology, 67(3–4), 317–334, doi:10.1016/j.geomorph.2004.10.007, 2005.

Swithinbank, C., Brunk, K. and Sievers, J.: A glaciological map of Filchner-Ronne ice shelf, Antarctica, Ann. Glaciol, 11, 150–155, 1988.

Thomas, R. H., MacAyeal, D. R., Eilers, D. H. and Gaylord, D. R.: Glaciological studies on the Ross ice shelf, Antarctica,
1035   1973–1978, Wiley Online Library. [online] Available from:
http://onlinelibrary.wiley.com/doi/10.1029/AR042p0021/summary (Accessed 28 October 2016), 1984.

Tinto, K. J., Padman, L., Siddoway, C. S., Springer, S. R., Fricker, H. A., Das, I., Tontini, F. C., Porter, D. F., Frearson, N. P.,
Howard, S. L., Siegfried, M. R., Mosbeux, C., Becker, M. K., Bertinato, C., Boghosian, A., Brady, N., Burton, B. L., Chu,
W., Cordero, S. I., Dhakal, T., Dong, L., Gustafson, C. D., Keeshin, S., Locke, C., Lockett, A., O'Brien, G., Spergel, J. J.,
1040   Starke, S. E., Tankersley, M., Wearing, M. G. and Bell, R. E.: Ross Ice Shelf response to climate driven by the tectonic
imprint on seafloor bathymetry, Nature Geoscience, 12(6), 441, doi:10.1038/s41561-019-0370-2, 2019.

Todd, C., Stone, J., Conway, H., Hall, B. and Bromley, G.: Late Quaternary evolution of Reedy Glacier, Antarctica, Quaternary
Science Reviews, 29(11–12), 1328–1341, doi:10.1016/j.quascirev.2010.02.001, 2010.

Webster, J., Hawes, I., Downes, M., Timperley, M. and Howard-Williams, C.: Evidence for regional climate change in the
1045   recent evolution of a high latitude pro-glacial lake, Antarctic Science, 8(1), 49–59, doi:10.1017/S0954102096000090,
1996.

van Wessem, J. M., Reijmer, C. H., Morlighem, M., Mouginot, J., Rignot, E., Medley, B., Joughin, I., Wouters, B., Depoorter,
M. A., Bamber, J. L., Lenaerts, J. T. M., Berg, W. J. V. D., Broeke, M. R. V. D. and Meijgaard, E. V.: Improved
representation of East Antarctic surface mass balance in a regional atmospheric climate model, Journal of Glaciology,
1050   60(222), 761–770, doi:10.3189/2014JoG14J051, 2014.

Whillans, I. M. and Merry, C. J.: Analysis of a shear zone where a tractor fell into a crevasse, western side of the Ross Ice
Shelf, Antarctica, Cold Regions Science and Technology, 33(1), 1–17, doi:10.1016/S0165-232X(01)00024-6, 2001.